Published in final edited form as:

J Comp Neurol. 2020 August ; 528(12): 2068–2098. doi:10.1002/cne.24877.

Wiring patterns from auditory sensory neurons to the escape and song-relay pathways in fruit flies

Hyunsoo Kim[1,3], **Mihoko Horigome**[1,3], **Yuki Ishikawa**[1], **Feng Li**[2], **J. Scott Lauritzen**[2], **Gwyneth Card**[2], **Davi D. Bock**[2,†], **Azusa Kamikouchi**[1,#]

[1]Graduate School of Science, Nagoya University, Chikusa, Nagoya, Aichi, 464-8602, Japan;

[2]HHMI Janelia Research Campus, Ashburn, VA, USA

[3]These authors equally contributed to this work.

Abstract

Many animals rely on acoustic cues to decide what action to take next. Unraveling the wiring patterns of the auditory neural pathways is prerequisite for understanding such information processing. Here we reconstructed the first step of the auditory neural pathway in the fruit fly brain, from primary to secondary auditory neurons, at the resolution of transmission electron microscopy. By tracing axons of two major subgroups of auditory sensory neurons in fruit flies, low-frequency tuned Johnston's organ (JO)-B neurons and high-frequency tuned JO-A neurons, we observed extensive connections from JO-B neurons to the main second-order neurons in both the song-relay and escape pathways. In contrast, JO-A neurons connected strongly to a neuron in the escape pathway. Our findings suggest that heterogeneous JO neuronal populations could be recruited to modify escape behavior whereas only specific JO neurons contribute to courtship behavior. We also found that all JO neurons have postsynaptic sites at their axons. Presynaptic modulation at the output sites of JO neurons could affect information processing of the auditory neural pathway in flies.

Graphical Abstract

[#]Correspondence should be addressed to A.K. (kamikouchi@bio.nagoya-u.ac.jp).
[†]Current address: Department of Neurological Sciences, University of Vermont, Burlington, VT, USA

Data availability statement

The data that support the findings of this study are available from the corresponding author upon request.

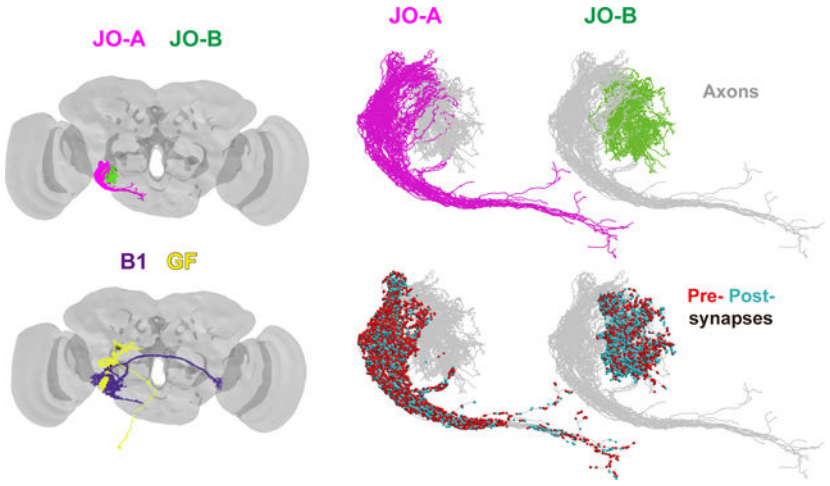

Using a high-resolution dataset of electron microscopy images of a fruit fly brain, we traced the axons of two major subgroups of auditory sensory neurons, JO-A and JO-B, and major downstream neurons, AMMC-B1 and GF, in the song-relay and escape pathways, respectively. JO-A and JO-B neurons have abundant pre- and post-synapses along their axons. Specific types of JO-A and JO-B neurons feed into the AMMC-B1 and/or GF pathways.

Keywords

Auditory neural pathway; courtship song; escape; electron microscopy; RRID: BDSC_25752; RRID: BDSC_39348; RRID: BDSC_40588; RRID: BDSC_52807; RRID: BDSC_25752; RRID: BDSC_77124; RRID: BDSC_28845; RRID: BDSC_52272; RRID: AB_10013483; RRID: AB_528108; RRID: AB_2338362; RRID: AB_141761; RRID: AB_141725

1 INTRODUCTION

Sound informs many animals about the environments they encounter. Noises from a predator trigger escape behavior, whereas love songs from a potential mating partner enhance mating behavior. How are these sounds processed in the brain? Elucidating the organization of auditory neural pathways is prerequisite to answering this question. Fruit flies are a useful model for mapping neural circuits at single-cell resolution because, in principle, all cells are genetically identifiable and manipulable at the single-cell level. Previous analyses of fruit flies using light microscopy (LM) revealed the projection patterns of auditory sensory neurons (Ishikawa et al., 2017; Kamikouchi et al., 2006) and secondary auditory neurons (Matsuo et al., 2016; Vaughan et al., 2014) in the brain at single-cell resolution. Information on the synapse distribution and connection patterns between auditory sensory neurons and secondary auditory neurons at the single-cell level, however, is still lacking, thereby limiting our understanding of the circuit organization between sensory and secondary auditory neurons. The recent development of a high-resolution dataset of electron microscopy (EM) images of the entire brain of an adult female fly, the whole-brain EM volume (Zheng et al., 2018), offers great potential for elucidating the organization of auditory neural pathways in the fly brain at synaptic resolution.

Fruit flies, *Drosophila melanogaster* and related species, utilize acoustic signals for intraspecific communications (Shorey, 1962). During courtship, a courting male generates acoustic signals by vibrating his wings. This sound, the so-called courtship song, has a species-specific temporal pattern and is important for species recognition (Cobb et al., 1989; Ewing & Bennet-Clark, 1968; Ewing & Manning, 1967). Fruit flies detect sounds with their antennal ear, comprised of the sound receiver and the mechanosensory organ, the so-called Johnston's organ (JO). The JO is housed in the second antennal segment and contains approximately 480 chordotonal neurons (Kamikouchi et al., 2006). These neurons, JO neurons, are classified into five subgroups according to their axonal projection targets in the brain and response properties. Among them, subgroup-A and subgroup-B JO neurons (JO-A and JO-B neurons hereafter) are classified as the major auditory sensory neurons, as they respond selectively to antennal vibrations (Kamikouchi et al., 2009). JO-A and JO-B neurons feed into two major categorical pathways; the song-relay pathway and escape pathway (Tootoonian et al., 2012; Vaughan et al., 2014), which include the antennal mechanosensory and motor center (AMMC)-B1 neurons (also described as aPN1 neurons; Vaughan et al., 2014) and giant fiber (GF) neurons, respectively. Indeed, these neurons are activated by sound stimuli (Tootoonian et al., 2012), and silencing AMMC-B1 neurons suppresses the fly's behavioral response to the courtship song (Vaughan et al., 2014; Yamada et al., 2018) while silencing GF neurons suppresses the looming-induced escape behavior (von Reyn et al., 2014). How JO-A and JO-B neurons each connect to these two types of downstream neurons, however, remains unknown. In this study, to clarify the synaptic connection pattern between auditory JO neurons and the song-relay and escape pathways, we traced individual JO-A and JO-B neuron axons, but not other three subgroups of JO neurons (JO- C, D, and E), at the synaptic resolution level using the whole-brain EM volume of an adult fly (4×4 nm resolution and sectioned at 40 nm thickness; Zheng et al., 2018; Li et al., 2019). Our findings provide insight into the organization of output synapses from individual JO neurons to the major song-relay and escape pathways, as well as abundant synaptic inputs to JO neuronal axons, which would regulate the spatiotemporal activity of JO neuron axons.

2 MATERIALS AND METHODS

2.1 Animals

Drosophila melanogaster fruit flies were used for all the experiments. EM imaging data were obtained from the brain of a 7-day-old *[iso]* w^{1118} *x [iso] Canton-S* G1 adult female fly as reported previously (Zheng et al., 2018). For immunohistochemistry, *En-GAL4* (RRID: BDSC_25752), *R74C10-GAL4* (RRID: BDSC_39348), *R91G04-GAL4* (RRID: BDSC_40588), *nSyb-GAL4* (Khuong et al., 2010), and *R68A06-LexA* (RRID: BDSC_52807) were used as driver strains. *UAS-2xEGFP* combined with *En-GAL4* (RRID: BDSC_25752) was used to visualize *En-GAL4* neurons. The *trans*-Tango strain (RRID: BDSC_77124) (Talay et al., 2017) was used to visualize neurons postsynaptic to JO neurons. To evaluate *nSyb-GAL4* expression in the GF neurons, *nSyb-GAL4* (Khuong et al., 2010) and *R68A06-LexA* were combined with *UAS-Stinger* (RRID: BDSC_28845) and *13XLexAop2-6XmCherry-HA* (RRID: BDSC_52272) strains, respectively.

2.2 Neuron tracing and reconstruction

To elucidate the connectivity between the auditory JO neurons and the song-relay and escape pathways, we traced JO-A, JO-B, AMMC-B1, and GF neurons using the EM image dataset of an adult fly brain. The EM imaging data comprised 7062 serial frontal sections (Zheng et al., 2018) that were collected anterior to posterior. It should be noted that the EM dataset used in this study was derived from one fly brain. We reconstructed neurons located on the right side of the brain by tracing neurites and annotated synapses using CATMAID (http://www.catmaid.org) (Schneider-Mizell et al., 2016). All neurons were reconstructed by two team members: HK and MH served as tracer and proofreader, respectively. Trace errors, comprising false-negatives and false-positives, were detected by the proofreader and corrected by the tracer. Total error rates (total length of traced neuron / the sum of false-negatives and false-positives) for neurite tracing by the tracer were 106.7 μm/error for JO-A neurons, 78.9 μm/error for JO-B neurons, and 199.9 μm/error for AMMC-B1 neurons. These error rates are comparable to those reported for an adult *Drosophila* brain using the same image dataset (Zheng et al., 2018). The GF neuron was traced independently (Card, in preparation).

We followed previously established criteria for identifying chemical synapses that included at least three of the four following features, with the first as an absolute requirement: (1) an active zone with vesicles; (2) presynaptic specialization such as a ribbon or T-bar; (3) synaptic clefts; and (4) postsynaptic membrane specialization such as postsynaptic densities (Zheng et al., 2018; Figure 1b). We did not attempt to identify electrical synapses (gap junctions) because they are unlikely to be resolved at the resolution of this dataset (Zheng et al., 2018). Therefore, only the chemical synaptic connections were analyzed in this study. EM tracing of the GF neuron was performed by Card and colleagues. To identify the AMMC, wedge (WED), and gnathal ganglia (GNG) neuropil, we used a surface model of neuropil compartments (Zheng et al., 2018). Raw length was utilized as neurite length for each reconstructed neuron.

2.3 Tracing of JO neuron axons

The cell bodies of JO neurons are in the second antennal segment, from where the axons project to the AMMC in the brain via the antennal nerve (Kamikouchi et al., 2006). After entering the brain, JO neuron axons project from the anterior side toward the posterior side of the brain and terminate mainly in the AMMC. The criteria used for identifying JO neuron axons were as follows: (1) at the anterior portion of the brain, the neurites were located within the AMMC and from there projected toward the posterior edge of the AMMC, and (2) cell bodies were not found in the brain. In this study, therefore, information about the cell body positions of traced JO neurons was not included. JO-A neuron axons were identified as having a neuronal trajectory located at the lateral side of the AMMC, with some sending branches projecting to the WED and/or GNG, and others terminating at the lateral posterior side of the AMMC, namely AMMC zone A (Kamikouchi et al., 2006; Ishikawa et al., 2017). JO-B neuron axons were identified as having a trajectory medial to the JO-A fascicle and within the lateral AMMC, namely AMMC zone B (Kamikouchi et al., 2006). These neurons separate from the JO-A fascicle as they pass the ventrolateral side of the antennal lobe (Kamikouchi et al., 2006). The total number of JO-A and JO-B neurons has not been

identified, but estimations from our previous reports suggest that each subgroup contains approximately 100 cells (Kamikouchi et al., 2006; Ishikawa et al., 2017). We therefore traced 45 JO-A and 45 JO-B neurons, which likely covers approximately half of the total population (Kamikouchi et al., 2006). As it was difficult to trace JO neuron axons from the forefront of the brain, we started our tracing at section #1400; that is, 1400 sections (~56 μm) posterior from the front of the brain, with the depth of the whole fly brain from this EM imaging data being around 250 μm and section #1 corresponding to the front of the antennal lobe. We first traced a candidate JO neuron toward its distal end and judged whether it fulfilled the criteria for being defined as either a JO-A or a JO-B neuron. If it was judged as either a JO-A or a JO-B neuron, we traced the identified JO neuron retrogradely from the starting point to the anterior side of the brain to obtain as complete a reconstruction as possible. Total axon lengths of traced JO-A (n=45) and JO-B (n=45) neurons, which included all the branches, were 12.9 mm and 8.0 mm, respectively. The starting section used to calculate axon length was set at section #1245 for JO-A neurons and #1423 for JO-B neurons (Table 12) to account for differences in the most anterior section of each JO neuron we traced. Presynaptic sites were densely distributed throughout the axons of both JO-A and JO-B neurons (Figures 2, 3), consistent with our previous report showing a broad distribution of presynaptic markers along the axons of JO-A and JO-B neurons (Kamikouchi et al., 2006). To determine a typical distribution pattern of pre- and post-synapses in each JO neuron axon (Figure 3), we randomly selected three JO-A neurons and four JO-B neurons (one neuron per type of JO-A and JO-B neuron defined in Table 9). Each JO-A or JO-B neuron was named in a serial manner (JO-A-1 to JO-A-45, JO-B-1 to JO-B-45) based on the number of synapses to the GF neuron and AMMC-B1 neurons found in this EM dataset. For JO-A neurons, type-1 JO-A neurons were numbered from JO-A-1 to JO-A-14 according to the number of output synapses to the GF, and type-3 JO-A neurons to the number of output synapses to AMMC-B1. For JO-B neurons, type-1 JO-B neurons were numbered from JO-B-1 to JO-B-11 according to the number of output synapses to the GF, and type- 2 and 3 JO-B neurons to the number of output synapses to AMMC-B1 (JO-B-12 to JO-B-24 and JO-B-25 to JO-B-32, respectively). Type-2 JO-A neurons and type-4 JO-B neurons (JO-A-15 to JO-A-43 and JO-B-33 to JO-B-45) had no synapses to the GF and AMMC-B1, and thus were numbered according to the order of axon tracing. Number of pre- and post-synapses, axon length, and density of pre- and post-synapses for each JO neuron are shown in Table 1.

2.4 Tracing of AMMC-B1 and GF neurons

Identification of AMMC-B1 neurons was based on their characteristic anatomy, including the somata location, trajectory of the neurons, and where they terminated (Matsuo et al., 2016). We began the AMMC-B1 tracings around section #3360, from where the AMMC neurite branches off the neurites that project to the ipsilateral WED, contralateral WED, and ipsilateral AMMC. We traced 5 AMMC-B1 neurons, which covered about half of the total population of ~10 neurons per side (Lai et al., 2012). Consistent with a previous report (Matsuo et al., 2016), two AMMC-B1 neurons innervated the ipsilateral GNG in addition to the ipsilateral AMMC and the WED on both sides of the brain (AMMC-B1–1, AMMC-B1–2; mean neurite length = 3.1 mm), whereas the other three did not (AMMC-B1–3, AMMC-B1–4, AMMC-B1–5; mean neurite length = 1.7 mm). The total neurite length of the traced AMMC-B1 neurons was 11.3 mm. The JFRC2013-to-EM volume transformation (Zheng et

al., 2018) confirmed that the traced neurons were classified as AMMC-B1 neurons identified at the confocal microscopic level (Kamikouchi et al., 2009; Lai et al., 2012; Vaughan et al., 2014). The GF neuron was traced and proofread to completion by Card and colleagues (Card, in preparation).

2.5 Immunohistochemistry

Immunolabeling was performed in female flies as described previously (Yamada et al., 2018). Briefly, brains were fixed with 4% paraformaldehyde in phosphate-buffered saline for 60 min on ice and subjected to antibody labeling. Primary antibodies used in this study were as follows: Rabbit anti-DsRed (Living Colors DsRed Polyclonal Antibody, Clontech, Mountain View, CA, #632496; RRID: AB_10013483; 1:1000 dilution) was used for detecting mtdTomato and mCherry signals. This antibody is rabbit antisera raised against DsRed-Express, a variant of *Discosoma* red fluorescent protein, and recognizes DsRed variants including DsRed2, mCherry, and tdTomato (manufacturer's notes). Rat anti-GFP IgG2a (nacalai tesque INC., Catalog# 04404–26; 1:1000 dilution) was used for detecting myrGFP, EGFP, and Stinger signals. This antibody was raised against His-GFP (full length) fusion protein and detects specifically GFP and GFP-fusion proteins (manufacturer's notes). Mouse anti-Bruchpilot nc82 (Developmental Studies Hybridoma Bank, Iowa City, IA, #nc82; RRID: AB_528108; 1:20 dilution) was used to visualize neuropils in the brain. It is a mouse monoclonal antibody that recognizes the ubiquitously expressed active zone protein, Bruchpilot, which forms protein bands of 170 and 190 kDa in Western blots of homogenized *Drosophila* heads (Wagh et al., 2006). The immunoreactive signal disappeared in the tissue as well as in the Western blots in RNAi-mediated Bruchpilot knockdown flies, and an additional up-shifted band was detected specifically if GFP-tagged Bruchpilot was expressed in a pan-neuronal manner (Wagh et al., 2006).

Secondary antibodies used in this study were as follows: Alexa Flour 488-conjugated anti-rat IgG (Jackson ImmunoResearch, Cambridgeshire, UK, #112-545-167; RRID: AB_2338362; 1:300 dilution), Alexa Fluor 555-conjugated anti-rabbit IgG (Invitrogen, #A21429, RRID: AB_141761; 1:300 dilution), and Alexa Fluor 647-conjugated anti-mouse IgG (Invitrogen, #A21236; RRID: AB_141725; 1:300 dilution).

2.6 Confocal microscopy and image processing

Serial optical sections of brains were obtained with a resolution of 512 × 512 pixels using an FV-1000D or FV3000 laser-scanning confocal microscope (Olympus, Tokyo, Japan) equipped with a silicone-oil immersion lens (30x objective, NA = 1.05, UPLSAPO30XS, 0.83 μm/pixel, 0.93-μm intervals; 60x objective, NA = 1.30, UPLSAPO60XS, 0.26 μm/pixel, 0.55-μm intervals; Olympus, Japan). Confocal datasets were reconstructed using the three-dimensional (3D)-reconstruction software FluoRender (Wan et al., 2009). For the projection analysis of En^+ JO neurons (Figure 8b), signals of cells that were not relevant to the traced neurons were erased manually from the original images utilizing FluoRender for clarity. To overlay the *trans*-Tango signals from different brain samples (Figure 14b), brain images were digitally aligned to a template brain with non-rigid registration using the Computational Morphometry Toolkit (CMTK; RRID: SCR_002234) (Jefferis et al., 2007). We used the signal of the nc82 antibody, which labels synaptic sites of all the neurons, as a

reference. The size and color of the images were adjusted using Photoshop CS5 (Adobe Systems, San Jose, CA; RRID: SCR_014198), FluoRender, and ImageJ (National Institutes of Health; RRID: SCR_003070).

2.7 Statistical analysis

Statistical analysis was performed using R (version 3.5.1) and RStudio (version 1.1.463). The mean and standard deviation (SD) were obtained with the mean and sd functions in R, respectively. Statistical tests and scores were listed in Supplementary tables 1–17. The result of $p < 2.2e\text{-}16$ indicates that the p value is very small. Because type-3 JO-A comprises only two neurons, we did not include them in the statistical tests except for the Supplementary tables 7 and 8. A significance level of $p < 0.05$ was used for all statistical tests, in which Bonferroni correction was used for multiple comparisons.

3 RESULTS

3. 1 Differences in the fine anatomy of JO-A and JO-B neurons

JO-A and JO-B axons innervate distinct brain targets, zones A and B, respectively, in the AMMC (Kamikouchi et al., 2006). We traced the axons of JO-A and JO-B neurons from their entrance into the brain (anterior side of the AMMC) to their terminus and mapped the synaptic sites along the axons (n = 45/JO subgroup; Figure 1; Supplementary Figures 1, 2; Table 1). JO-A neurons had longer axon lengths (286.8 ± 114.9 μm *vs* 177.2 ± 31.2 μm; p = 4.15e-07) and more presynaptic sites than JO-B neurons (896 ± 344 *vs* 329 ± 89; p < 2.2e-16) (Table 2; Supplementary tables 1, 2). The density of presynaptic sites was also higher in JO-A neuron axons than JO-B neuron axons (3.1 ± 0.6 presynaptic sites/μm in JO-A neurons and 1.9 ± 0.6 presynaptic sites/μm in JO-B neurons; p < 2.2e-16; Supplementary table 3).

Postsynaptic sites were also identified in both JO-A and JO-B axons (Figures 2, 3; Supplementary Figures 1, 2). All traced JO neuron axons had postsynaptic sites, but the number of postsynaptic sites was not strongly correlated with that of presynaptic sites in either the JO-A or JO-B neuronal subgroups (rs = 0.20, p = 0.19 for JO-A; r = −0.07, p = 0.69 for JO-B; Supplementary table 4). JO-A neuron axons had more postsynaptic sites than JO-B neuron axons (93 ± 27 in JO-A *vs* 81 ± 27 in JO-B postsynaptic sites per neuron; p = 0.04; Table 2; Supplementary table 5), but the density was lower than that in JO-B neuron axons (0.3 ± 0.17 postsynaptic sites/μm in JO-A neurons *vs* 0.5 ± 0.16 postsynaptic sites/μm in JO-B neurons; p = 0.005; Supplementary table 6).

Some JO neuron axons made synaptic contacts with each other: 13 JO-A neurons contacted other JO-A neurons (15 synapses in total, corresponding to 0.36% of total postsynaptic sites in JO-A neuron axons); 21 JO-B neurons contacted other JO-B neurons (30 synapses in total, corresponding to 0.82% of total postsynaptic sites in JO-B neuron axons); but no synapses between JO-A and JO-B neurons were observed (Tables 2–7). The majority of synaptic inputs to JO-A and JO-B neuron axons came from unidentified (untraced) neurons (Tables 4, 7), although it is possible that some of the untraced neurons were untraced JO neuron axons. The distribution of postsynaptic sites was broad and intermingled with

presynaptic sites along the axons of the JO neurons (Figures 2, 3; Supplementary Figures 1, 2).

3.2 Contacts between JO neurons and song-relay and escape pathways

We previously identified interneurons that presumably connect with JO-A and JO-B neurons at the LM level (Kamikouchi et al., 2009; Matsuo et al., 2016). Among them, AMMC-B1 and GF neurons are second-order neurons, each of which has a central role in the song-relay and escape pathways (Allen et al., 2006; Lai et al., 2012; von Reyn et al., 2014; Yamada et al., 2018). In each side of the brain, AMMC-B1 neurons form a cluster of approximately 10 neurons each that connect the ipsilateral AMMC zone B and WED (Kamikouchi et al., 2009; Lai et al., 2012). GF neurons comprise a pair of large descending neurons, one in each side of the brain, whose cell bodies lie in the posterior brain with dendrites innervating the ipsilateral AMMC zones A and B, posterior ventrolateral protocerebrum, gorget, and inferior clamp, and whose axons project to the thoracico-abdominal ganglion (Power, 1948; Matsuo et al., 2016). To quantitatively examine the synaptic contacts of JO-A and JO-B neurons to these pathways, we traced AMMC-B1 and GF neurons (n = 5 and n = 1, respectively; Figure 4a). Among the five AMMC-B1 neurons we traced, two innervated the GNG whereas the other three did not (Figure 4b). These two AMMC-B1 neurons that innervated the GNG (termed AMMC-B1–1 and AMMC-B1–2) had more branches and longer neurite lengths than those of the other three AMMC-B1 neurons (AMMC-B1 −3, −4, and −5; Table 8). This anatomical heterogeneity of AMMC-B1 neurons corresponds well with a previous report describing the anatomy of single AMMC-B1 neurons at the LM level (Matsuo et al., 2016).

Mapping synapses between auditory sensory neurons (JO-A and JO-B neurons) and second-order neurons (AMMC-B1 and GF neurons) revealed their distinct connection patterns (Figure 5; Tables 3–7). AMMC-B1 neurons received inputs almost exclusively from JO-B neurons and rarely from JO-A neurons; 4% of JO-A (2/45) and 47% of JO-B neurons (21/45) had output synapses to AMMC-B1 neurons (Figure 5a, left). On the other hand, the GF neuron received many inputs from both JO-A and JO-B neurons: 31% of JO-A (14/45) and 53% of JO-B neurons (24/45) had synaptic contacts to the GF neuron (Figure 5a, right). This biased contribution pattern was more obvious when evaluating the number of synapses among each of these neurons: AMMC-B1 neurons received 3 synapses from 2 JO-A neurons, but 587 synapses from 21 JO-B neurons, whereas the GF neuron received 690 synapses from 14 JO-A neurons and 251 synapses from 24 JO-B neurons (Figure 5; Table 9). This indicates that both JO-A and JO-B neurons send information to the GF neuron, whereas the AMMC-B1 neurons receive signals mainly from JO-B neurons. Among the AMMC-B1 neurons, the number of synapses from JO neurons varied; a single AMMC-B1 neuron received a mean of 118 synapses from traced JO neurons, but there was a 1.6-fold difference between the five traced AMMC-B1 neurons (Table 8). This variance did not seem to correlate with the morphological differences among AMMC-B1 neurons. Notably, the AMMC-B1 and GF neurons had no synaptic output to JO neurons (Figure 5b), suggesting that there is no direct monosynaptic feedback via chemical synapses from these second-order neurons to JO neurons.

Besides AMMC-B1 and GF neurons, all JO-A and JO-B neurons have abundant synaptic outputs to unidentified neurons; JO-A and JO-B neuron axons have 39,600 and 13,940 output synapses (98% and 94% of all synapses), respectively, onto unidentified neurons (Figure 5b; numbers of synapses from individual JO-A and JO-B neurons to unidentified neurons are shown in Tables 3, 5). This suggests that AMMC-B1 and GF neurons are minor direct targets of synaptic transmissions from JO-A and JO-B neurons. Likewise, most of the synaptic inputs to JO-A and JO-B neurons originate from unidentified neurons; JO-A and JO-B neuron axons receive 4187 and 3632 synaptic inputs from unidentified neurons, respectively, which is a far greater number than that of synaptic inputs from JO neurons (Figure 5b; numbers of synapses from unidentified neurons to individual JO-A and JO-B neuron axons are shown in Tables 4, 7).

3.3 A specific JO-A neuron type connects to the GF neuron

Previous LM studies revealed morphological and physiological heterogeneities among JO-A neurons (Kamikouchi et al., 2006; Ishikawa et al., 2017). To reveal the connection pattern between such heterogeneous JO-A and GF neurons at the EM level, we classified JO-A neurons according to the number of synapses with each of the AMMC-B1 neurons and GF neuron. This analysis clearly divided EM-traced JO-A neurons into three types: type-1 neurons with many synaptic outputs to the GF neuron (14/45), type-2 neurons with no connections to the traced AMMC-B1 and GF neurons (29/45), and type-3 neurons that synapse to AMMC-B1 neurons (2/45) (Table 9). Axons of type-1 JO-A neurons were confined within the AMMC, whereas those of type- 2 and 3 JO-A neurons had one or two long branches that branched out from the main axon bundle that projects within the AMMC and innervated the WED and/or GNG (Figures 6, 7). Thus, a specific type of JO-A neuron, whose projections are confined within the AMMC, transmits information to the GF escape pathway. Notably, we observed no JO-A neurons projecting to both AMMC-B1 and GF, suggesting that AMMC-B1 and GF neurons each receives input from distinct type of JO-A neurons. Pre- and post- synaptic sites are located more anteriorly in type-1 JO-A than in type- 2 and 3 ($p < 2.2e-16$; Figure 7; Supplementary tables 7, 8), but the distribution of synaptic sites shows no obvious variations between individual JO-A neurons of the same type (Supplementary Figure 1).

Only type- 1 and 2 JO-A neurons make synaptic contacts with other JO-A neurons, and all of these synapses are within the same type of JO-A neurons; 10 synapses between type-1 and 5 synapses between type-2 JO-A neuron axons (Tables 10, 11). Although we found only two JO-A neurons that synapse to AMMC-B1, both of them connected to a specific AMMC-B1 neuron (Table 9). This AMMC-B1 neuron (here termed AMMC-B1–4) had the smallest number of branches (280 branches) and received the smallest number of synapses from JO-B neurons among AMMC-B1 neurons (Table 8). Type- 2 and 3 JO-A neurons innervate the more posterior side of the brain ($p < 2.2e-16$ between types 1 and 2) and have longer axons than type-1 JO-A neurons ($p = 2.55e-11$ between types 1 and 2; Table 12; Supplementary tables 9, 10). Axon length corresponded well with the number of presynaptic sites, but not with the number of postsynaptic sites ($rs = 0.86$ and 0.02, $p = 2.04e-14$ and 0.90, respectively; Supplementary table 11). The number of postsynaptic sites of type-2 JO-A neurons ranged widely, from 43 to 143 per neuron (Table 1).

Our EM results show that type-1 JO-A neurons, which innervate only within the AMMC, connect to the GF neuron via chemical synapses; 8.6% of type-1 JO-A neuron output synapses were connected to the GF neuron (690 synapses from type-1 JO-A neurons to the GF neuron in total). A previous study showed that JO-A neurons expressing the transcription factor Engrailed (En) (En^+ JO-A neurons hereafter) form mixed electrical and chemical synaptic inputs onto GF dendrites (Pézier et al., 2014). To investigate whether the anatomical characteristics of En^+ JO-A neurons are consistent with those of type-1 JO-A neurons, we analyzed the projection patterns of En^+ JO-A neurons in the brain. As reported previously, En^+ JO-A axons innervate zones A, B, and E in the AMMC. In zone A, En^+ JO-A axons innervate only within the AMMC, and not outside it (i.e., WED and GNG; Figure 8). This innervation pattern of En^+ JO-A axons corresponds closely with that of type-1 JO-A neurons, which have many synaptic outputs to the GF neuron (Table 9). Although our EM analysis identified only the chemical synapses, these results together suggest that type-1 JO-A neurons that transmit signals to the GF neuron can be identified by En expression, with transmission being mediated by both chemical and electrical synapses.

3.4 JO-B neurons can project to both the escape and song-relay pathways

In contrast to JO-A neurons, many JO-B neurons (13/45) showed synaptic outputs to both AMMC-B1 and GF neurons. Analysis of output-synapse numbers onto AMMC-B1 and GF neurons classified JO-B neurons into four types: type-1 neurons with synaptic output to the GF neuron but not to AMMC-B1 neurons (11/45), type-2 neurons with connections to both AMMC-B1 and GF neurons (13/45), type-3 neurons with connections to AMMC-B1 neurons but not to the GF neuron (8/45), and type-4 neurons with no connections to either the traced AMMC-B1 neurons or the GF neuron (13/45) (Table 9). Type-4 JO-B neurons, however, exhibited many synaptic outputs to unidentified neurons (as observed in type-2 JO-A neurons), confirming that many JO-A and JO-B neurons feed into neural pathways other than the AMMC-B1 and GF pathways (Figure 5b; Tables 3, 5, 6, 13). Although the total axon lengths were similar between all types (Table 12; $p = 0.56$; Supplementary table 12), axonal projections of type- 1 and 2 JO-B neurons, which have connections to the GF, located more laterally, terminated more anteriorly, and had more postsynaptic sites than those of type- 3 and 4 JO-B neurons (Figures 9, 10; Table 12; Supplementary tables 13, 14). No obvious morphological differences in the axons were detected between either type- 1 and 2 or type- 3 and 4 JO-B neurons. Notably, many JO-B neurons (21/45) made connections with other JO-B neurons, and most of the connections were between JO-B neurons of the same type (Tables 5–7, 10, 14). This within-type connection property is similar to that of JO-A neurons, suggesting that the synaptic connections within each neuronal type could be a general property of JO neurons. The distributions of the synaptic sites along the anterior-posterior axis of the brain differed between types, except for between types 1 and 2, but no obvious variations were observed between individual JO-B neurons of the same type (Figure 10; Supplementary Figure 2; Supplementary tables 15, 16).

Type-2 JO-B neurons make the majority of synaptic connections with AMMC-B1 neurons (500 of 587 synapses in total from JO-B to AMMC-B1 neurons; Table 15). Most type-2 JO-B neurons (9/13, named JO-B-12 to JO-B-20) had more than 30 synapses to AMMC-B1 neurons, all of which had synaptic outputs to all of the traced AMMC-B1 neurons (Table 9).

Presumably, these JO-B neurons could send signals to all AMMC-B1 neurons as well as to the GF neuron. In contrast, type-3 JO-B neurons, which connect to AMMC-B1 neurons but not to the GF neuron, have a biased connection pattern to the five traced AMMC-B1 neurons. Two AMMC-B1 neurons (AMMC-B1–1 and AMMC-B1–2) received most of the synaptic contacts, whereas the other three AMMC-B1 neurons (AMMC-B1–3, AMMC-B1–4, and AMMC-B1–5) received only a few synaptic inputs from type-3 JO-B neurons (Table 15). Anatomically, AMMC-B1–1 and AMMC-B1–2 neurons had a long branch to the GNG, whereas the other AMMC-B1 neurons did not (Figure 4b), suggesting a specific function of AMMC-B1–1 and AMMC-B1–2 neurons in transmitting signals from type- 2 and 3 JO-B neurons to the GNG and WED.

3.5 Synaptic regions of AMMC-B1 and GF neurons

Five AMMC-B1 neurons, AMMC-B1–1 to −5, were heterogeneous with respect to the number of branches, neurite length, and number of synapses from JO neurons (Table 8). We found, however, that these distinct types of AMMC-B1 neurons received synaptic inputs from JO-B neurons at similar regions of their neurites in AMMC zone B (Figures 11, 12). On the other hand, the synaptic locations on AMMC-B1 neurons varied depending on the JO-B neuron type. Type-2 JO-B neurons synapsed to the anterior-lateral part of the AMMC-B1 dendrites, whereas type-3 JO-B neurons typically synapsed to the posterior-medial part of the AMMC-B1 dendrites (Figures 11, 12). This segregation of synaptic regions corresponded well with the distinct regions of type- 2 and 3 JO-B axons in AMMC zone B, in which axons of type-2 JO-B innervated more laterally and terminated more anteriorly than those of type-3 JO-B axons (Figures 9, 10, Table 12). Synapses from JO-A neurons were distributed more laterally, where AMMC zone A is located, than those of JO-B neurons (Figures 2, 11, 12). Together, these observations suggest that the dendritic region of AMMC-B1 neurons can be divided into several domains, each receiving input from a specific type of JO-A and JO-B neurons.

In contrast, the synaptic sites of type- 1 and 2 JO-B neurons were intermingled on the branches of the GF neuron (Figure 13), consistent with their axonal distributions. Although synapses from JO-A neurons were distributed more laterally than those of JO-B neurons, the dendritic region of the GF neuron was unlikely to be divided by input sites from specific types of JO-B neurons.

3.6 Analysis of synaptic connections with *trans*-Tango

To evaluate whether the synaptic connections between JO neurons and AMMC-B1 and GF neurons are detectable by molecular genetic tools at the LM level, we used *trans*-Tango (Talay et al., 2017), a tool used to identify monosynaptic downstream neurons. *R74C10-GAL4* and *R91G04-GAL4*, which label most JO-A (Ishikawa et al., 2017) and JO-B neurons, respectively, were used to drive the expression of *trans*-Tango. Both *GAL4* drivers strongly labeled AMMC-B1 neurons, indicating synaptic connections between AMMC-B1 neurons and JO-A/JO-B neurons (Figure 14a). Moreover, the numbers of AMMC-B1 neurons labeled as monosynaptic downstream neurons were different between JO-A and JO-B neurons: 4.7 ± 2.4 AMMC-B1 neurons were postsynaptic to JO-A (*R74C10-GAL4* > *trans*-Tango; n = 9), whereas 10.9 ± 2.6 AMMC-B1 neurons were postsynaptic to JO-B

(*R91G04-GAL4* > *trans*-Tango; n = 8). AMMC-B1 neurons labeled by both *GAL4* drivers were spatially overlapped and shared the typical branching pattern of AMMC-B1 neurons (Kamikouchi et al., 2009) (Figure 14b). Taken together, JO-B neurons had more AMMC-B1 neurons than JO-A neurons as their monosynaptic downstream neurons ($p < 2.2e-16$; Supplementary table 17), which validates the findings from our EM tracing. On the other hand, neither of them labeled GF neurons as being postsynaptic to JO-A and JO-B neurons (Figure 14a). We found that the pan-neuronal driver *nSyb-GAL4* (Khuong et al., 2010) did not label GF neurons (Figure 14c), suggesting that the "pan-neuronal" cassettes in *trans*-Tango are not expressed in GF neurons. Together, this result confirmed the EM tracing result showing that both JO-A and JO-B neurons have synaptic connections to AMMC-B1 neurons. It also demonstrates the need for careful interpretation of anatomical data using molecular genetic tools, which mostly rely on the fidelity of the promoter activities.

4 DISCUSSION

In the present study, we performed a sparse reconstruction of JO-A, JO-B, and AMMC-B1 neurons, in which approximately half of each neuronal population was reconstructed. For JO-A and JO-B neurons, all the pre and postsynaptic sites located in the brain were identified. Subsequently, all the synapses from traced JO-A and JO-B neurons to AMMC-B1 neurons were mapped. Together with the tracing data of the GF neuron that was reconstructed completely with all the pre- and post- synapse distribution patterns identified (Card, et al in preparation), we revealed the fine organization of JO neurons that contribute to the song-relay and escape pathways. We also revealed that AMMC-B1 and GF neurons are minor direct targets of synaptic transmissions from JO-A and JO-B neurons, as most of the synaptic connections were found between these JO neurons and unidentified neurons. The sign of synapses (excitatory or inhibitory) and dynamic properties cannot be determined by the EM images (Takemura et al., 2008) and thus the properties of the synapses are difficult to be estimated.

4.1 Anatomy of JO-A and JO-B neuron axons

A previous study at the LM level revealed the heterogeneity of JO-A neurons (Ishikawa et al., 2017). Anatomically, at least 20 types of JO-A neurons have been identified, each of which has a specific combination of projection target regions in the brain (Kamikouchi et al., 2006; Ishikawa et al., 2017). These 20 types of JO-A neurons identified at the LM level can be classified into either of the three types identified in the present study; type-1 JO-A neurons represent JO-AA, AP, and AA/AP neurons in the previous classification, and type- 2 and 3 JO-A neurons correspond with the other JO-A neurons that innervate the WED and/or GNG in addition to AMMC zone A. Such correspondence suggests the consistency between the LM and EM analyses. The previous study at the LM level revealed that JO-A neurons labeled with *R88B12-GAL4* are mostly JO-AP neurons (Ishikawa et al., 2017) whose projections are confined within AMMC zone A and therefore mostly comprise the type-1 JO-A neurons identified in this study. These neurons responded maximally to vibrations with a frequency of 100 to 200 Hz when tested with pure tones from 40 to 800 Hz (Ishikawa et al., 2017). Acoustic signals within the 100 to 200 Hz frequency range could therefore maximally activate type-1 JO-A neurons and be transmitted to the downstream GF neuron.

On the other hand, there is a clear discrepancy in the results of the LM and EM analyses of JO-B neuron branching patterns. A previous LM study reported that some JO-B neurons have a single ending while others have multiple endings at the distal side of their projections (Kamikouchi et al., 2006). Here, however, we found that all JO-B neurons had multiple endings with “twigs”, which are defined as short and microtubule-free terminal branches (Schneider-Mizell et al., 2016). This discrepancy is likely due to the limited spatial resolution of the LM analysis; the size of the twigs is as fine as 40 nm in diameter (Zheng et al., 2018), which would preclude detection by LM. It is therefore necessary to re-examine the morphology of single neurons at the EM level to reveal their detailed anatomy.

Extensive contacts between JO neuron axons, including putative gap junctions, were reported previously (Sivan Loukianova and Eberl, 2005). In the present study, which identified only the chemical synapses, we found that some JO-A and JO-B neurons have synaptic connections with other JO neurons. Interestingly, most of these connections are confined within the same type in either JO-A or JO-B neurons (Table 10). Because JO neurons are cholinergic (Ishikawa et al., 2017), such axo-axonic synapses within the same type of JO neurons might excite the partner neuron and could therefore facilitate auditory information transmission to the same downstream neurons. Of note, olfactory sensory neurons of the fruit fly that project to the same glomerulus also have chemical synapses between their axons (Tobin et al., 2017). Further studies are needed to elucidate how these axo-axonic chemical synapses affect the transmission properties of sensory neurons.

4.2 Song-relay pathway

AMMC-B1 neurons are the major secondary auditory neurons so far identified that relay song information to downstream neurons. Indeed, silencing AMMC-B1 neurons suppresses female receptivity for copulation in response to the courtship song (Vaughan et al., 2014; Yamada et al., 2018). Anatomically, AMMC-B1 neurons connect the ipsilateral AMMC zone B, where JO-B neurons project, and the WED on both sides of the brain (Kamikouchi et al., 2009). Our EM tracing revealed that the majority of auditory inputs to AMMC-B1 neurons originated from JO-B neurons. A few synaptic inputs from JO-A neurons to a specific AMMC-B1 neuron were observed, however, in our EM tracing and confirmed by the *trans*-Tango experiment, suggesting that JO-A neurons also partly contribute to AMMC-B1 activity. This JO-B neuron dominance in the song-relay pathway is consistent with findings from previous reports that JO-B neurons are necessary for the fly’s song response (Kamikouchi et al., 2009), whereas JO-A neurons contribute but are not necessary (Ishikawa et al., 2017). Taken together, we conclude that JO-B neurons are the main auditory sensory neurons that relay song information to AMMC-B1 neurons. JO-A neurons also feed into this major song-relay pathway, but their contribution is smaller than that of JO-B neurons. Notably, AMMC-B1 neurons have heterogeneous connection patterns. Although all of them receive synaptic input from type-2 JO-B neurons almost equally, two AMMC-B1 neurons that have a long branch innervating the GNG (AMMC-B1–1 and AMMC-B1–2) intensively receive additional input from type-3 JO-B neurons. AMMC-B1 neurons can therefore be divided into two types according to their innervation of the GNG, which strongly correlates with synaptic input from type-3 JO-B neurons. An AMMC-B1 neuron with a long branch to

the GNG may have a distinct function by transmitting signals from type-3 JO-B neurons to the GNG.

It should be noted that the connections from JO-A neurons to AMMC-B1 neurons revealed by our EM tracing were very weak (3 synapses). Because the EM dataset used in this study is based on a single female fly, the reliability of such weak connections should be carefully evaluated. In this study, the *trans*-Tango experiment validated the synaptic connections from JO-A neurons to AMMC-B1 neurons. A combination of LM- and EM-based experiments will be useful for evaluating connections with a few synapses.

4.3 Escape pathway

GF neurons, also known as giant descending neurons, are a bilateral pair of large descending neurons whose activation induces an escape takeoff in flies (Power, 1948; Lima and Miesenböck, 2005; von Reyn et al., 2014). In *Drosophila* as well as larger fly species, visual stimuli and mechanical stimulation of the antenna activate GF neurons (Bacon and Strausfeld, 1986; Mu et al., 2014). In *Drosophila*, sound pulse stimulation induces graded responses in GF neurons (Tootoonian et al., 2012; Lehnert et al., 2013). Taken together, GF neurons should process visual and acoustic information that would control the escape behavior of flies, although it is not clear whether auditory stimuli modulate the looming-evoked escape response of *Drosophila*.

The GF neuron innervates AMMC zones A and B as well as three other neuropil in the ipsilateral brain before sending out a long axon to the thoracico-abdominal ganglion to terminate on jump muscle motor neurons (Bacon and Strausfeld, 1986; Matsuo et al., 2016). Our EM tracing revealed that the GF neuron receives many synaptic inputs from both JO-A and JO-B neurons, but only specific types of JO-A or JO-B neurons feed into the GF escape pathway. Type-1 JO-A neurons, which were classified by their synaptic contact to the GF neuron, have rather uniform axons confined within the AMMC and terminate more anteriorly than other types of JO-A neurons (Table 12). Two other types of JO-A neurons, type- 2 and 3, have branches projecting to other neuropil (WED and/or GNG). Such distinct anatomical differences between type-1 and the other two types of JO-A neurons, together with the specific connection to the GF neuron, suggest a function of type-1 JO-A neurons to influence escape behavior in flies.

In contrast to JO-A neurons, the JO-B types are morphologically similar but differ in the depth of their axonal projections. A previous flip-out analysis using confocal microscopy revealed JO-B neurons with short-type or long-type axons (Kamikouchi et al., 2006). Correspondingly, our EM tracing revealed that axons of type- 1 and 2 JO-B neurons terminated more anteriorly than those of type- 3 and 4 JO-B neurons in the brain. Having an anterior-terminated, and thus proximal-terminated, axon is a common characteristic of JO neurons that have synaptic output to the GF escape pathway, which drives a short-duration escape takeoff evoked by a single GF spike (von Reyn et al., 2014). In crickets, acoustic stimuli modulate their escape responses evoked by airflow stimuli (Fukutomi and Ogawa, 2017). The findings from that study and ours together suggest that the auditory input could modulate avoidance behaviors in response to other sensory stimuli both in crickets and flies.

A subset of JO-A neurons express the transcription factor En and make both gap junctions and chemical synapses with the GF neuron (Pézier et al., 2014). Axons of these En^+ JO-A neurons correspond well with those of type-1 JO-A neurons (Figure 8). Type-1 JO-A neurons and En^+ JO-A neurons could be the same set of JO neurons that sends signals to GF neurons via a mixture of gap junctions and chemical synapses.

4.4 JO neurons for song-relay and escape pathways

Many animals rely on acoustic cues from the environment to detect predators and mating partners. The auditory system must be able to discriminate the nature of sound signals to make an immediate appropriate behavioral response. Cricket ears have two hearing ranges peaking at lower sonic and ultrasonic frequencies, which correspond to mating and predator sounds, respectively (Hedwig and Stumpner, 2016). Crickets show categorical processing of frequencies, e.g., positive phonotaxis to the sonic-range sound and negative phonotaxis (escape) to ultrasonic signals emitted by predatory bats (Wyttenbach et al., 1996). On the other hand, the frequency range detected by the fruit-fly antennal ear is estimated to be lower than ~1000 Hz (Goepfert and Hennig, 2016). In this narrow frequency range, frequencies of mating and predator sounds could overlap. Such ambiguous sounds should be evaluated in downstream auditory pathways, which requires neurons that transmit auditory information to both the song-relay and escape pathways.

Type-2 JO-B neurons are strong candidates for such neurons that transmit information to both pathways because they have synaptic outputs to both AMMC-B1 and GF neurons. These non-specific transmissions would activate both pathways when ambiguous sounds are detected by the antennal ear of fruit flies. The behavioral outputs of each pathway are regulated by signals of other sensory modalities (e.g., visual-looming stimulus for the escape pathway and pheromones for mating behavior) (von Reyn et al., 2014; Auer and Benton, 2016). Thus, auditory signals transmitted to both song-relay and escape pathways are likely to have a priming effect on these pathways, each of which could be turned on only when simultaneous inputs from the other sensory modalities are detected to trigger a specific behavior.

Previous reports suggest that spiders and ants are *Drosophila* predators (Soto-Yéber et al., 2018; Parigi et al., 2019). Indeed, *Drosophila* adults fly away upon the arrival of ants at prickly pear fruits (Soto-Yéber et al., 2018). Moreover, dragon flies are assumed to be predators of small flying insects such as mosquitoes and flies, and *Drosophila* is often used to feed dragon flies in laboratory conditions (Mischiati et al., 2015; Okude et al., 2017). Further behavioral studies of adult *Drosophila* in the wild will help to elucidate the ethological meaning of type-2 JO-B neurons projecting to both song-relay and escape pathways.

Here, we traced JO-A and JO-B neurons, but not the other three subgroups of JO neurons, namely JO- C, D, and E. It is thus possible that AMMC-B1 and GF neurons also receive synaptic inputs from these untraced JO neurons. Indeed, findings from a recent study suggest that AMMC-B1 neurons might be downstream of subgroup C and E JO neurons and contribute to the responses of WED projection neurons, which are excited by ipsilateral wind stimuli (Suver et al., 2019). Future studies to trace the other subgroups of JO neurons,

subgroups C, D, and E, as well as untraced JO-A and JO-B neurons, in this EM image dataset will be necessary to reconstruct the comprehensive wiring diagram between JO, AMMC-B1, and GF neurons.

4.5 JO neurons connected to other pathways

Most of the output synapses of JO-A and JO-B neuron axons connect to unidentified neurons in the brain, suggesting that various downstream pathways other than the AMMC-B1 and GF pathways are involved in acoustic information processing by fruit flies. Further studies will reveal complete circuit information downstream of these JO neurons.

4.6 Postsynaptic sites in JO neuron axons

We observed many postsynaptic sites in JO-A and JO-B neurons that are distributed broadly along the entire axons. Whereas some JO-A and JO-B neurons have synaptic contacts with other JO neurons, most of the postsynapses on JO-A and JO-B axons are from unidentified neurons in the brain (Figure 5b), strongly suggesting that the activity of JO neurons is modulated presynaptically in a centrifugal manner.

A candidate for such a modulator is the GABAergic system. In the olfactory system of fruit flies, presynaptic inhibition via GABA receptors in olfactory sensory neurons mediates gain control and temporal contrast enhancement in an olfactory circuit (Olsen and Wilson, 2008; Root et al., 2008; Raccuglia et al., 2016). In bush crickets, presynaptic inhibition mediated by GABAergic neurons from the central nervous system modulates the efficiency of synaptic transmission in auditory sensory neurons (Baden and Hedwig, 2010). Testing the expression of GABA receptors in JO-A and JO-B axons should be the first step toward exploring whether GABAergic signals from the central brain modulate the synaptic transmission of these JO neurons.

Intermingled distributions of presynaptic and postsynaptic sites are observed in various regions within the fruit-fly brain, i.e., the Kenyon cell dendrites in the mushroom body, and visual and olfactory neural circuits (Rybak et al., 2016; Takemura et al., 2017; Tobin et al., 2017; Zheng et al., 2018), as well as the auditory sensory neurons we observed in the present study. Such intermingled distributions of presynaptic and postsynaptic sites could be a general property of *Drosophila* neural circuits, which could contribute to the complex neuronal computations with a small number of neurons.

Supplementary Material

Refer to Web version on PubMed Central for supplementary material.

Acknowledgements

We thank A. Geens, P. Verstreken, K. Ito, and Bloomington *Drosophila* Stock Center for fly stocks, the Developmental Studies Hybridoma Bank for reagents, M. Kuno, Y. Maki, and Y. Ishikawa for fly maintenance, T. Kohashi, M. P. Su, A. Seeds, and S. Hampel for discussion, and J. Polsky, S. Alghailani, E. Tenshaw, R. Parekh, K. Eichler, S. A. Calle-Schuler, C. B. Fisher and I. J. Ali for the EM tracing. This work was supported by MEXT KAKENHI Grants-in-Aid for Scientific Research (B) (JP16H04655 to AK and JP18H02488 to YI), Scientific Research on Innovative Areas “Evolinguistics” (Grant JP18H05069 to AK), “Systems science of bio-navigation (Grant JP19H04933 to AK), and “Constrained and directional evolution” (Grant JP18H04819 to YI), Challenging

Research (Exploratory) (JP17K19450 to AK and JP17K19425 to YI), the Naito foundation to AK, and the HHMI Janelia Visiting Scientist Program to AK. HK, MH, and AK performed portions of this work as participants in the HHMI Janelia Visiting Scientist Program. HK was supported by an overseas research program for young scientists at Nagoya University.

References

Allen MJ, Godenschwege TA, Tanouye MA, Phelan P (2006). Making an escape: development and function of the *Drosophila* giant fibre system. Seminars in Cell and Developmental Biology 17:31–41. 10.1016/j.semcdb.2005.11.011 [PubMed: 16378740]

Auer TO, Benton R (2016). Sexual circuitry in *Drosophila*. Current Opinion in Neurobiology 38:18–26. 10.1016/j.conb.2016.01.004 [PubMed: 26851712]

Bacon JP, Strausfeld NJ (1986). The dipteran 'Giant fibre' pathway: neurons and signals. Journal of Comparative Physiology A 158:529–548. 10.1007/BF00603798

Baden T, Hedwig B (2010). Primary afferent depolarization and frequency processing in auditory afferents. The Journal of Neuroscience 30:14862–14869. 10.1523/JNEUROSCI.2734-10.2010 [PubMed: 21048145]

Cobb M, Burnet B, Blizard R, Jallon JM (1989). Courtship in *Drosophila sechellia*: Its structure, functional aspects, and relationship to those of other members of the *Drosophila melanogaster* species subgroup. Journal of Insect Behavior 2:63–89. 10.1007/BF01053619

Ewing AW, Bennet-Clark HC (1968). The courtship songs of *Drosophila*. Behaviour 31:288–301.

Ewing AW, Manning A (1967). The evolution and genetics of insect behaviour. Annual Review of Entomology 12:471–494.

Freifeld L, Clark DA, Schnitzer MJ, Horowitz MA, Clandinin TR (2013). GABAergic lateral interactions tune the early stages of visual processing in *Drosophila*. Neuron 78:1075–1089. 10.1016/j.neuron.2013.04.024 [PubMed: 23791198]

Fukutomi M, Ogawa H (2017). Crickets alter wind-elicited escape strategies depending on acoustic context. Scientific Reports 7:15158 10.1038/s41598-017-15276-x [PubMed: 29123249]

Göpfert MC, Hennig RM (2016). Hearing in insects. Annual Review of Entomology 61:257–276. 10.1146/annurev-ento-010715-023631

Harrison JB, Chen HH, Sattelle E, Barker PJ, Huskisson NS, Rauh JJ, Bai D, Sattelle DB (1996). Immunocytochemical mapping of a C-terminus anti-peptide antibody to the GABA receptor subunit, RDL in the nervous system of *Drosophila melanogaster*. Cell and Tissue Research 284:269–278. 10.1007/s004410050587 [PubMed: 8625394]

Hedwig B, Stumpner A (2016). Central neural processing of sound signals in insects In: Insect Hearing. Springer p 177–214.

Ishikawa Y, Kamikouchi A (2016). Auditory system of fruit flies. Hearing Research 338:1–8. 10.1016/j.heares.2015.10.017 [PubMed: 26560238]

Ishikawa Y, Okamoto N, Nakamura M, Kim H, Kamikouchi A (2017). Anatomic and physiologic heterogeneity of subgroup-A auditory sensory neurons in fruit flies. Frontiers in Neural Circuits 11:46 10.3389/fncir.2017.00046 [PubMed: 28701929]

Kamikouchi A, Inagaki HK, Effertz T, Hendrich O, Fiala A, Göpfert MC, Ito K (2009). The neural basis of *Drosophila* gravity-sensing and hearing. Nature 458:165–171. 10.1038/nature07810 [PubMed: 19279630]

Kamikouchi A, Shimada T, Ito K (2006). Comprehensive classification of the auditory sensory projections in the brain of the fruit fly *Drosophila melanogaster*. The Journal of Comparative Neurology 499:317–356. 10.1002/cne.21075 [PubMed: 16998934]

Khuong TM, Habets RLP, Slabbaert JR, Verstreken P (2010). WASP is activated by phosphatidylinositol-4, 5-bisphosphate to restrict synapse growth in a pathway parallel to bone morphogenetic protein signaling. Proceedings of the National Academy of Sciences of the United States of America 107:17379–17384. 10.1073/pnas.1001794107 [PubMed: 20844206]

Lai JS-Y, Lo S-J, Dickson BJ, Chiang A-S (2012). Auditory circuit in the *Drosophila* brain. Proceedings of the National Academy of Sciences of the United States of America 109:2607–2612. 10.1073/pnas.1117307109 [PubMed: 22308412]

Lehnert BP, Baker AE, Gaudry Q, Chiang A-S, Wilson RI (2013). Distinct roles of TRP channels in auditory transduction and amplification in *Drosophila*. Neuron 77:115–128. 10.1016/j.neuron.2012.11.030 [PubMed: 23312520]

Li PH, Lindsey LF, Januszewski M, Zheng Z, Bates AS, Taisz I, … Jain V (2019). Automated reconstruction of a serial-section EM *Drosophila* brain with flood-filling networks and local realignment. BioRxiv 605634 10.1101/605634

Lima SQ, Miesenböck G (2005). Remote control of behavior through genetically targeted photostimulation of neurons. Cell 121:141–152. 10.1016/j.cell.2005.02.004 [PubMed: 15820685]

Manning A (1967). The control of sexual receptivity in female *Drosophila*. Anim Behav 15:239–250. 10.1016/0003-3472(67)90006-1 [PubMed: 6030948]

Matsuo E, Seki H, Asai T, Morimoto T, Miyakawa H, Ito K, Kamikouchi A (2016). Organization of projection neurons and local neurons of the primary auditory center in the fruit fly *Drosophila melanogaster*. The Journal of Comparative Neurology 524:1099–1164. 10.1002/cne.23955 [PubMed: 26762251]

Mischiati M, Lin H-T, Herold P, Imler E, Olberg R, Leonardo A (2015). Internal models direct dragonfly interception steering. Nature 517:333–338. https://doi.org/10.1038/s41598-017-15276-x10.1038/nature1404510.1038/nature14045 [PubMed: 25487153]

Mu L, Bacon JP, Ito K, Strausfeld NJ (2014). Responses of *Drosophila* giant descending neurons to visual and mechanical stimuli. Journal of Experimental Biology 217(Pt 12):2121–2129. 10.1242/jeb.099135 [PubMed: 24675562]

Okude G, Futahashi R, Tanahashi M, Fukatsu T (2017). Laboratory rearing system for *Ischnura senegalensis* (Insecta: Odonata) enables detailed description of larval development and morphogenesis in dragonfly. Zoological Science 34:386–397. 10.2108/zs170051 [PubMed: 28990479]

Olsen SR, Wilson RI (2008). Lateral presynaptic inhibition mediates gain control in an olfactory circuit. Nature 452:956–960. 10.1038/nature06864 [PubMed: 18344978]

Pézier A, Jezzini SH, Marie B, Blagburn JM (2014). Engrailed alters the specificity of synaptic connections of *Drosophila* auditory neurons with the giant fiber. The Journal of Neuroscience 34:11691–11704. 10.1523/JNEUROSCI.1939-14.2014 [PubMed: 25164665]

Power ME (1948). The thoracico-abdominal nervous system of an adult insect, *Drosophila melanogaster*. The Journal of Comparative Neurology 88:347–409. 10.1002/cne.900880303 [PubMed: 18866775]

Raccuglia D, McCurdy LY, Demir M, Gorur-Shandilya S, Kunst M, Emonet T, Nitabach MN (2016). Presynaptic GABA receptors mediate temporal contrast enhancement in *Drosophila* olfactory sensory neurons and modulate odor-driven behavioral kinetics. eNeuro 3 10.1523/ENEURO.0080-16.2016

von Reyn CR, Breads P, Peek MY, Zheng GZ, Williamson WR, Yee AL, Leonardo A, Card GM (2014). A spike-timing mechanism for action selection. Nature Neuroscience 17:962–970. 10.1038/nn.3741 [PubMed: 24908103]

Root CM, Masuyama K, Green DS, Enell LE, Nässel DR, Lee C-H, Wang JW (2008). A presynaptic gain control mechanism fine-tunes olfactory behavior. Neuron 59:311–321. 10.1016/j.neuron.2008.07.003 [PubMed: 18667158]

Rybak J, Talarico G, Ruiz S, Arnold C, Cantera R, Hansson BS (2016). Synaptic circuitry of identified neurons in the antennal lobe of *Drosophila melanogaster*. The Journal of Comparative Neurology 524:1920–1956. 10.1002/cne.23966 [PubMed: 26780543]

Schneider-Mizell CM, Gerhard S, Longair M, Kazimiers T, Li F, Zwart MF, Champion A, Midgley FM, Fetter RD, Saalfeld S (2016). Quantitative neuroanatomy for connectomics in *Drosophila*. eLife 5:e12059 10.7554/eLife.12059 [PubMed: 26990779]

Shorey HH (1962). Nature of the sound produced by *Drosophila melanogaster* during courtship. Science 137:677–678. 10.1126/science.137.3531.677 [PubMed: 17770950]

Sivan-Loukianova E, Eberl DF (2005). Synaptic ultrastructure of *Drosophila* Johnston's organ axon terminals as revealed by an enhancer trap. The Journal of Comparative Neurology 491:46–55. 10.1002/cne.20687 [PubMed: 16127697]

Suver MP, Matheson AMM, Sarkar S, Damiata M, Schoppik D, Nagel KI (2019). Encoding of wind direction by central neurons in *Drosophila*. Neuron 102:828–842.e7. 10.1016/j.neuron.2019.03.012 [PubMed: 30948249]

Takemura S, Meinertzhagen IA (2008). Synaptic circuits of the *Drosophila* optic lobe: the input terminals to the medulla. The Journal of Comparative Neurology 509:493–513. 10.1002/cne.21757 [PubMed: 18537121]

Takemura S, Aso Y, Hige T, Wong A, Lu Z, Xu CS, Rivlin PK, Hess H, Zhao T, Parag T (2017). A connectome of a learning and memory center in the adult *Drosophila* brain. eLife 6:e26975 10.7554/eLife.26975 [PubMed: 28718765]

Talay M, Richman EB, Snell NJ, Hartmann GG, Fisher JD, Sorkaç A, Santoyo JF, Chou-Freed C, Nair N, Johnson M (2017). Transsynaptic mapping of second-order taste neurons in flies by trans-Tango. Neuron 96:783–795. e4. 10.1016/j.neuron.2017.10.011 [PubMed: 29107518]

Tobin WF, Wilson RI, Lee W-CA (2017). Wiring variations that enable and constrain neural computation in a sensory microcircuit. eLife 6:e24838 10.7554/eLife.24838 [PubMed: 28530904]

Tootoonian S, Coen P, Kawai R, Murthy M (2012). Neural representations of courtship song in the *Drosophila* brain. The Journal of Neuroscience 32:787–798. 10.1523/JNEUROSCI.5104-11.2012 [PubMed: 22262877]

Vaughan AG, Zhou C, Manoli DS, Baker BS (2014). Neural pathways for the detection and discrimination of conspecific song in *D. melanogaster*. Current Biology 24:1039–1049. 10.1016/j.cub.2014.03.048 [PubMed: 24794294]

Wagh DA, Rasse TM, Asan E, Hofbauer A, Schwenkert I, Dürrbeck H, Buchner S, Dabauvalle MC, Schmidt M, Qin G, Wichmann C, Kittel R, Sigrist SJ, Buchner E (2006). Bruchpilot, a protein with homology to ELKS/CAST, is required for structural integrity and function of synaptic active zones in *Drosophila*. Neuron 49:833–844. 10.1016/j.neuron.2006.02.008 [PubMed: 16543132]

Wan Y, Otsuna H, Chien CB, Hansen C (2009). An interactive visualization tool for multi-channel confocal microscopy data in neurobiology research. IEEE Transactions on Visualization and Computer Graphics 15:1489–1496. 10.1109/TVCG.2009.118 [PubMed: 19834225]

Wyttenbach RA, May ML, Hoy RR (1996). Categorical perception of sound frequency by crickets. Science 273:1542–1544. 10.1126/science.273.5281.1542 [PubMed: 8703214]

Yamada D, Ishimoto H, Li X, Kohashi T, Ishikawa Y, Kamikouchi A (2018). GABAergic local interneurons shape female fruit fly response to mating songs. The Journal of Neuroscience 38:4329–4347. 10.1523/JNEUROSCI.3644-17.2018 [PubMed: 29691331]

Zheng Z, Lauritzen JS, Perlman E, Robinson CG, Nichols M, Milkie D, Torrens O, Price J, Fisher CB, Sharifi N (2018). A complete electron microscopy volume of the brain of adult *Drosophila melanogaster*. Cell 174:730–743. e22. 10.1016/j.cell.2018.06.019 [PubMed: 30033368]

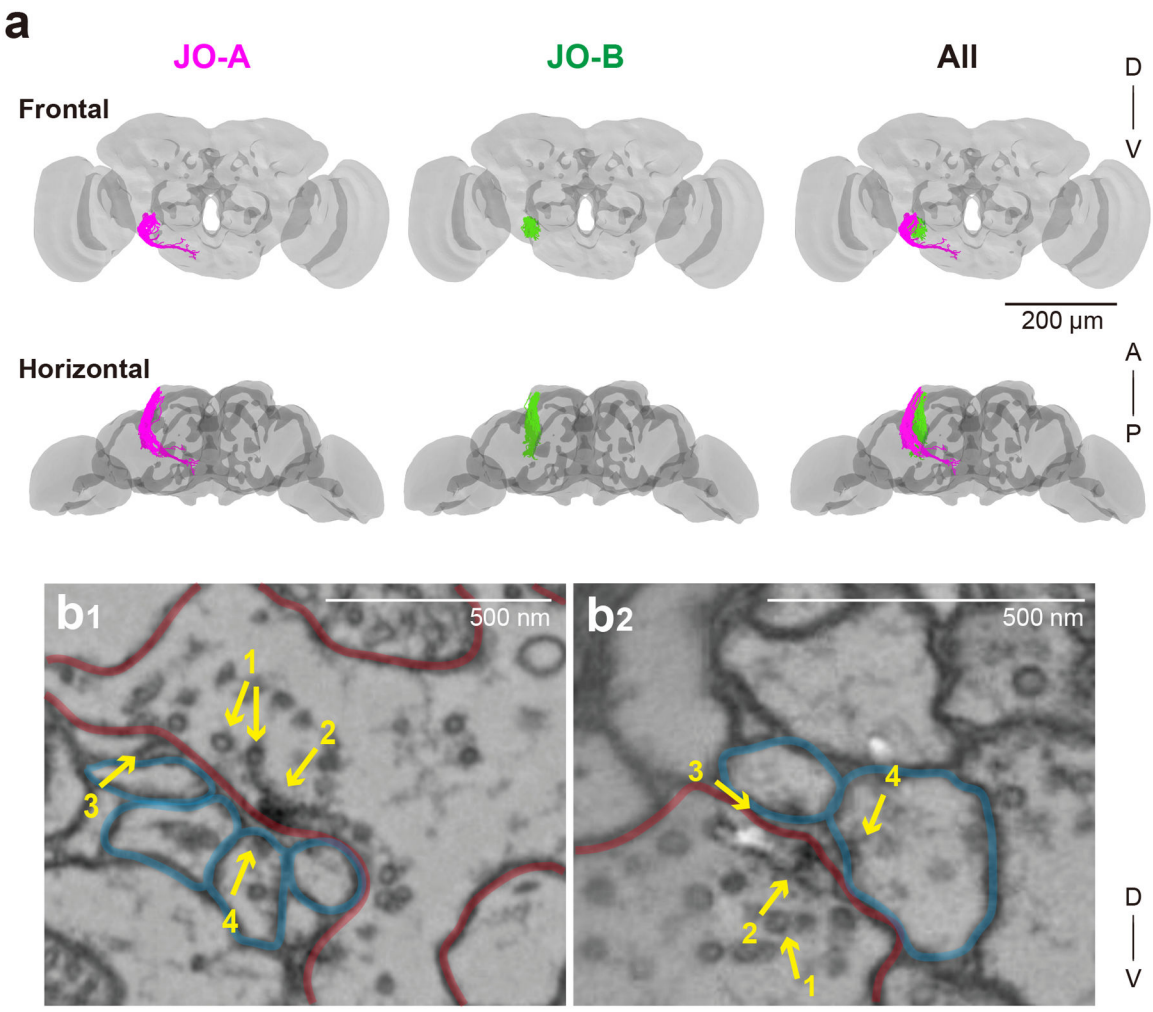

Figure 1 |. EM tracing of JO neuron axons

(a) 3D reconstructed images of 45 JO-A (magenta) and 45 JO-B neuron axons (green). Gray background shows the neuropil compartments of a whole brain (Zheng et al., 2018). A, anterior; D, dorsal; P, posterior; V, ventral. (b) Synapses of JO neurons visualized in the EM dataset. Pre- and post- synapses are outlined in red and blue, respectively. 1, synaptic vesicles; 2, T-bar; 3, synaptic cleft; 4, postsynaptic density.

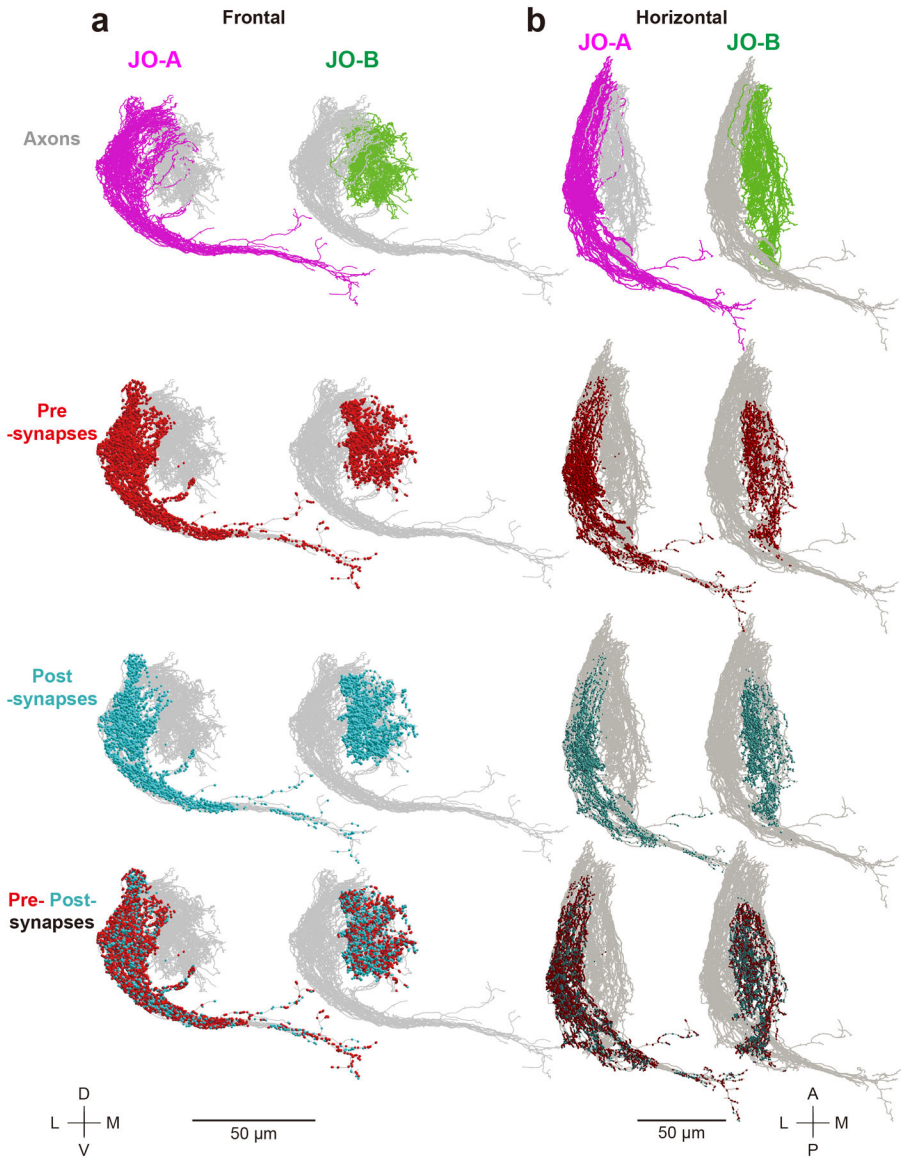

Figure 2 |. Summary of traced JO-A and JO-B neurons

Axons of traced JO-A (magenta) and JO-B (green) neurons, presynapses (red dots), and postsynapses (light blue dots) are shown (n = 45 for both JO-A and JO-B neurons). Frontal (a) and horizontal (b) views are shown. Gray background shows the axons of all the traced JO-A and JO-B neurons in this study. The upper side of the axons in the horizontal view (b) represents the proximal side of JO neuron axons. A, anterior; D, dorsal; L, lateral; M, medial; P, posterior; V, ventral.

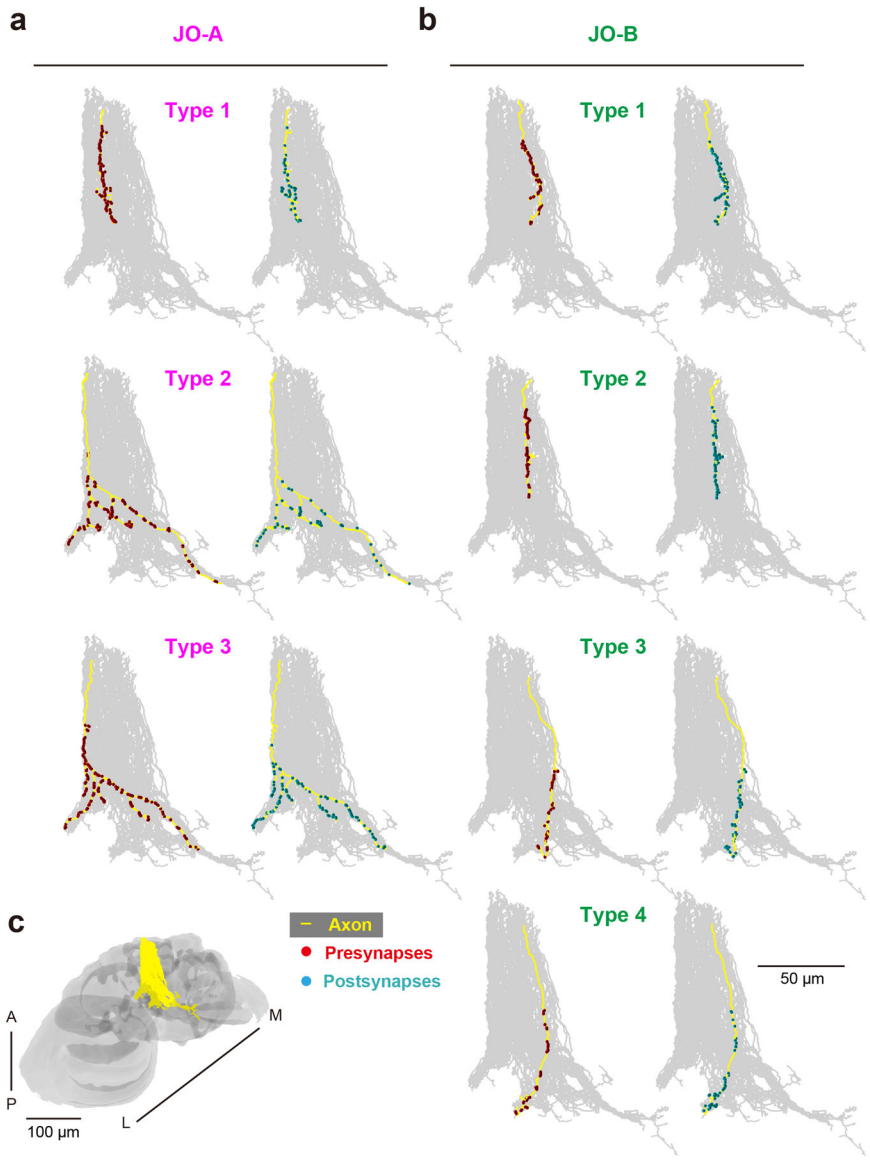

Figure 3 |. Synapse distributions along the axons of single JO-A and JO-B neurons

(a, b) Presynaptic sites (red) and postsynaptic sites (light blue) are intermingled along the axons of JO-A (a) and JO-B (b) neurons (yellow). Oblique views are shown. Gray background shows the axons of all the traced JO-A and JO-B neurons in this study. The upper side of the axons represents the proximal side of JO neuron axons. (c) Axons of all the traced JO-A and JO-B neurons (yellow) in the brain (gray). The angle of the brain is the same as that in panels a and b. Types of JO-A and JO-B are defined in Table 9. A, anterior; L, lateral; M, medial; P, posterior.

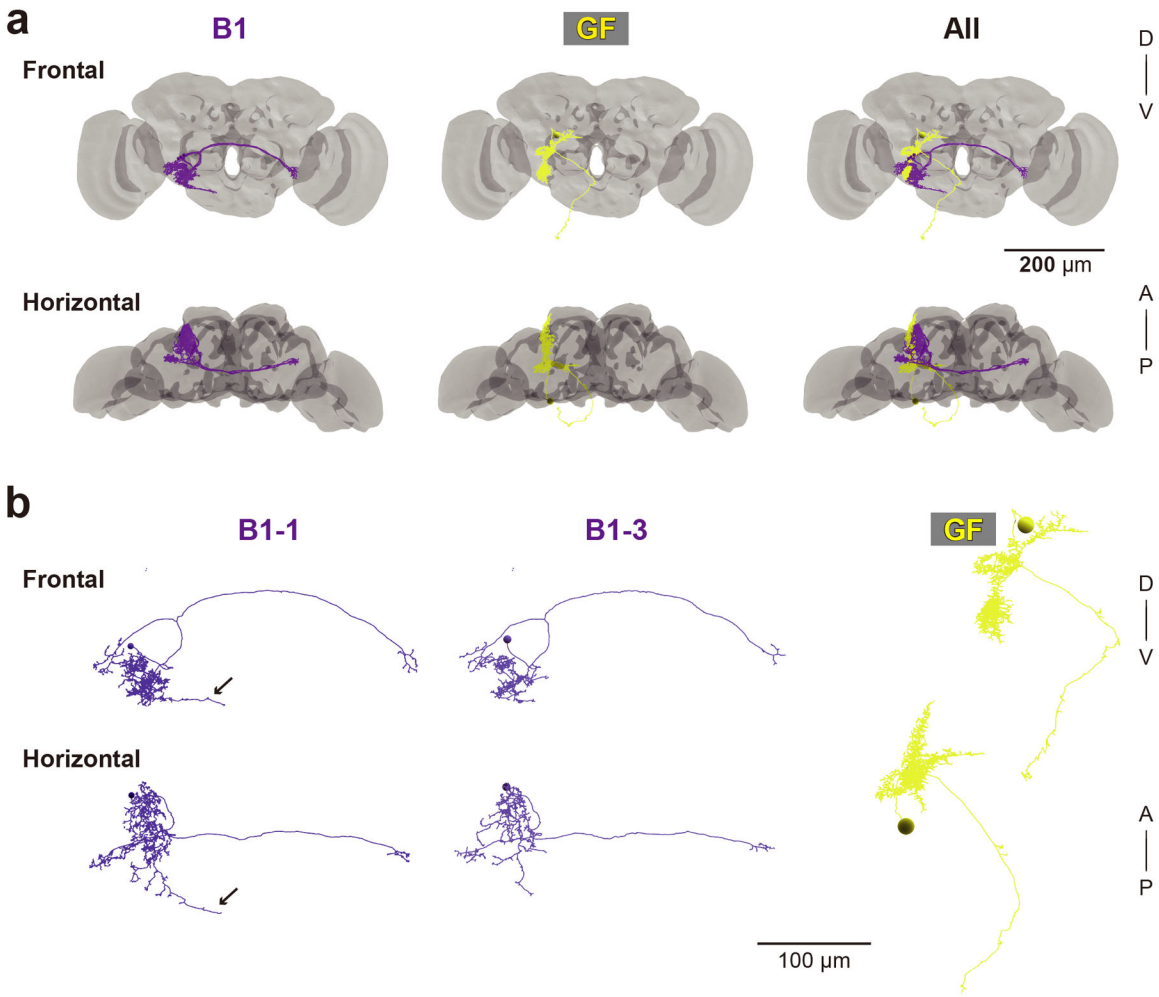

Figure 4 |. EM tracing of AMMC-B1 and GF neurons

(a) 3D reconstructed images of five AMMC-B1 neurons (B1, dark violet) and a GF neuron (GF, yellow). Gray backgrounds represent the neuropil of a fly brain (Zheng et al., 2018). (b) Reconstruction of AMMC-B1 and GF neurons. Arrows indicate the AMMC-B1 branches innervating the GNG (left). Each AMMC-B1 neuron is named serially (B1–1 to B1–5), in which only typical examples (AMMC-B1–1 and B1–3) are shown (left and middle). A, anterior; D, dorsal; P, posterior; V, ventral.

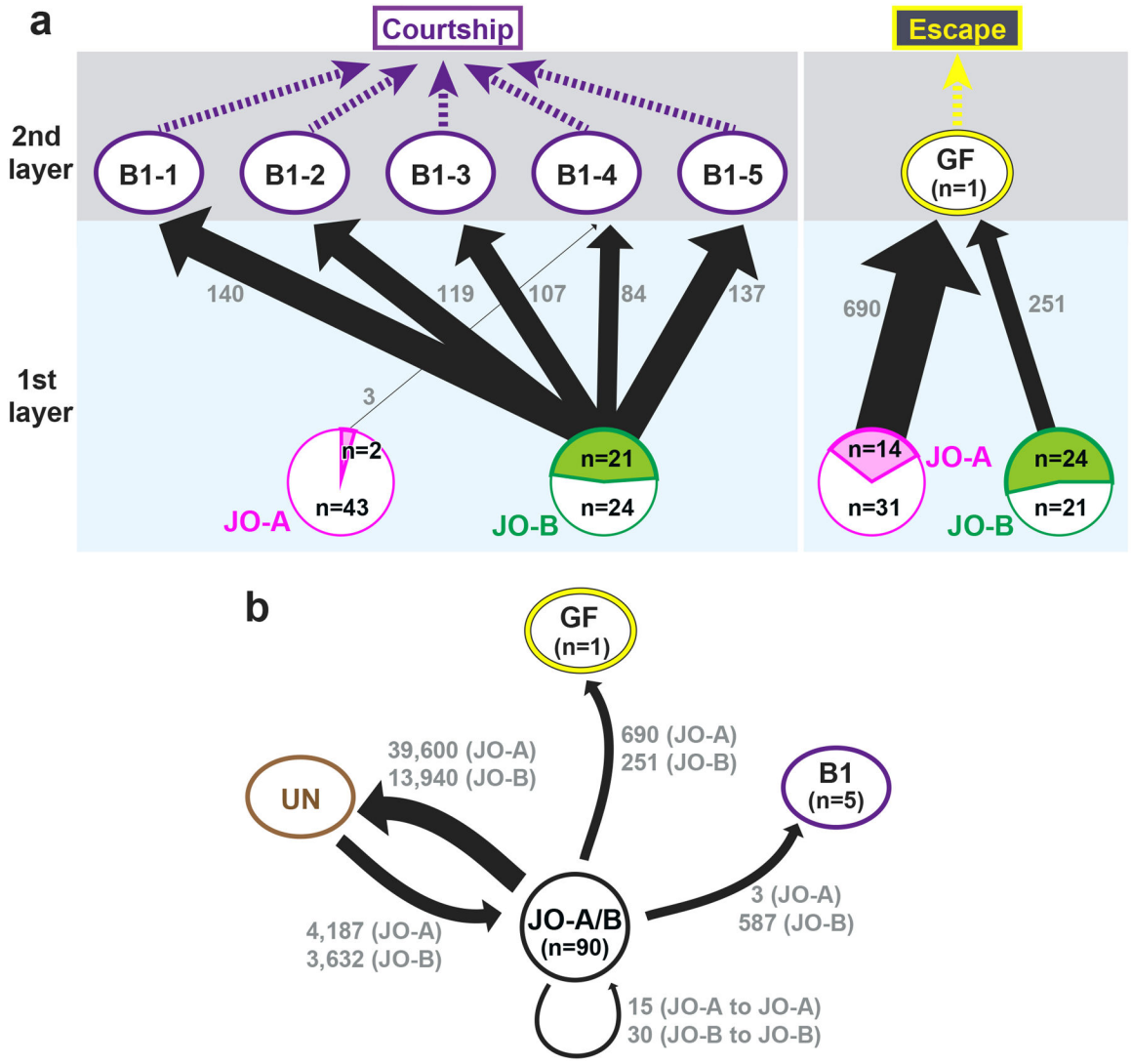

Figure 5 |. Synaptic connections of auditory neural pathways

(a) Connection diagram between JO neurons and the two pathways. The AMMC-B1 (B1) pathway, which feeds into the courtship-song relay pathway, receives many synaptic inputs from JO-B neurons and a few inputs from JO-A neurons (left). The GF pathway, which feeds into an escape pathway, receives many synaptic inputs from both JO-A and JO-B neurons (right). The arrow width reflects the number of synaptic connections. The number at each arrow (gray) indicates the number of synapses from JO neurons to each second-order neuron (AMMC-B1 or GF neuron). The magenta and green areas in JO-A and JO-B circles (bottom) represent the ratio of JO-A and JO-B neurons, respectively, that feed into AMMC-B1 (left) and GF neurons (right). The white area in each circle represents JO-A and JO-B neurons that have no output synapses to AMMC-B1 and GF neurons. “n” in the circle indicates the number of traced JO neurons that are connected (in magenta or green area) or not connected (in white area) to AMMC-B1 (left) and GF neurons (right). (b) Synaptic contacts between JO neurons and other neurons. JO-A and JO-B neuron axons receive many synaptic inputs from unidentified neurons (UN) but not from GF and AMMC-B1 neurons.

There are no synaptic contacts between JO-A and JO-B neurons. The number at each arrow shown in gray color indicates the number of synapses.

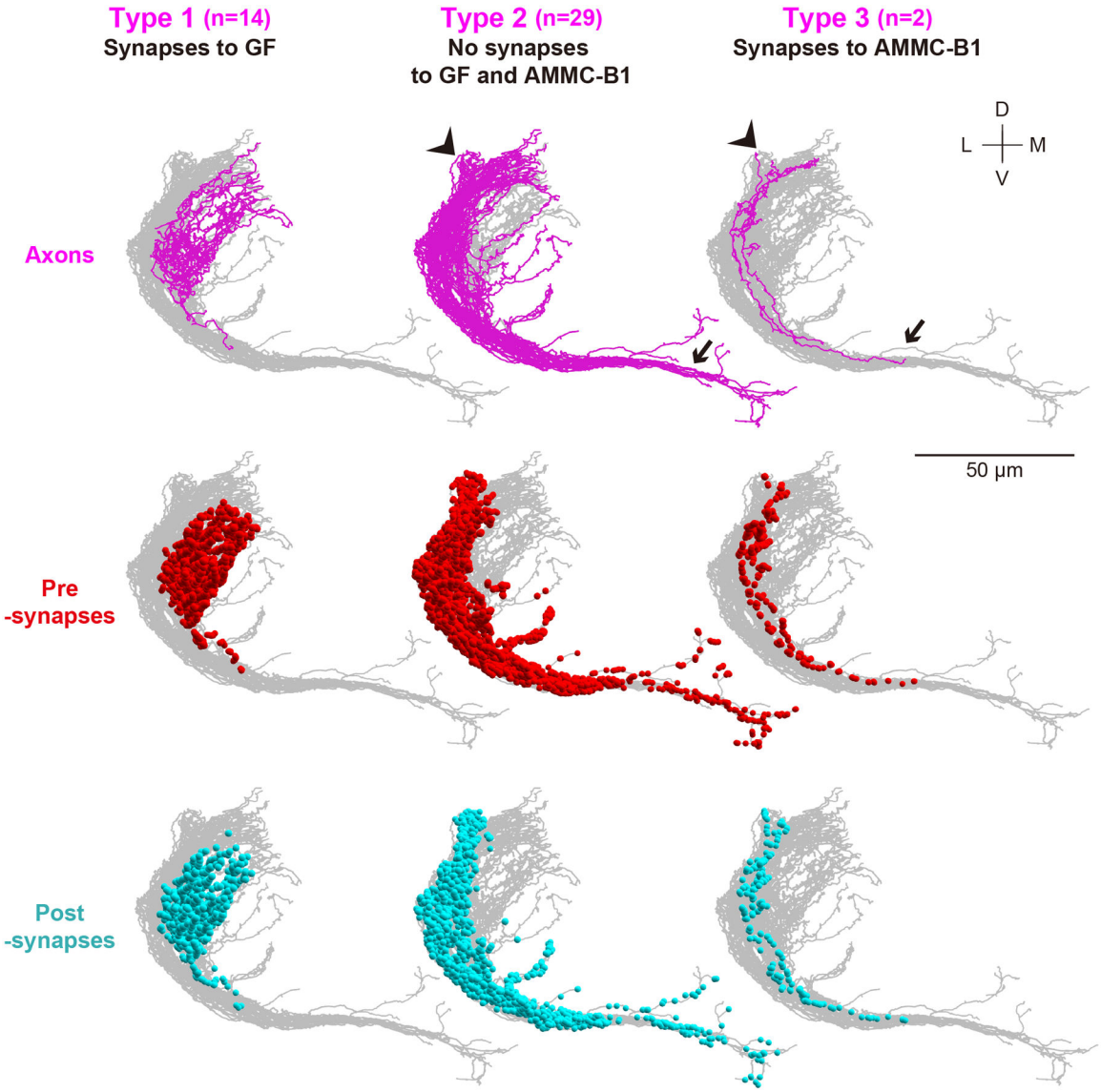

Figure 6 |. Three types of JO-A neurons

Frontal views of axons (magenta), presynapses (red dots), and postsynapses (light blue dots) are shown. The arrow and arrowhead indicate the axons of type- 2 and 3 JO-A neurons innervating the GNG and WED, respectively. D, dorsal; L, lateral; M, medial; V, ventral.

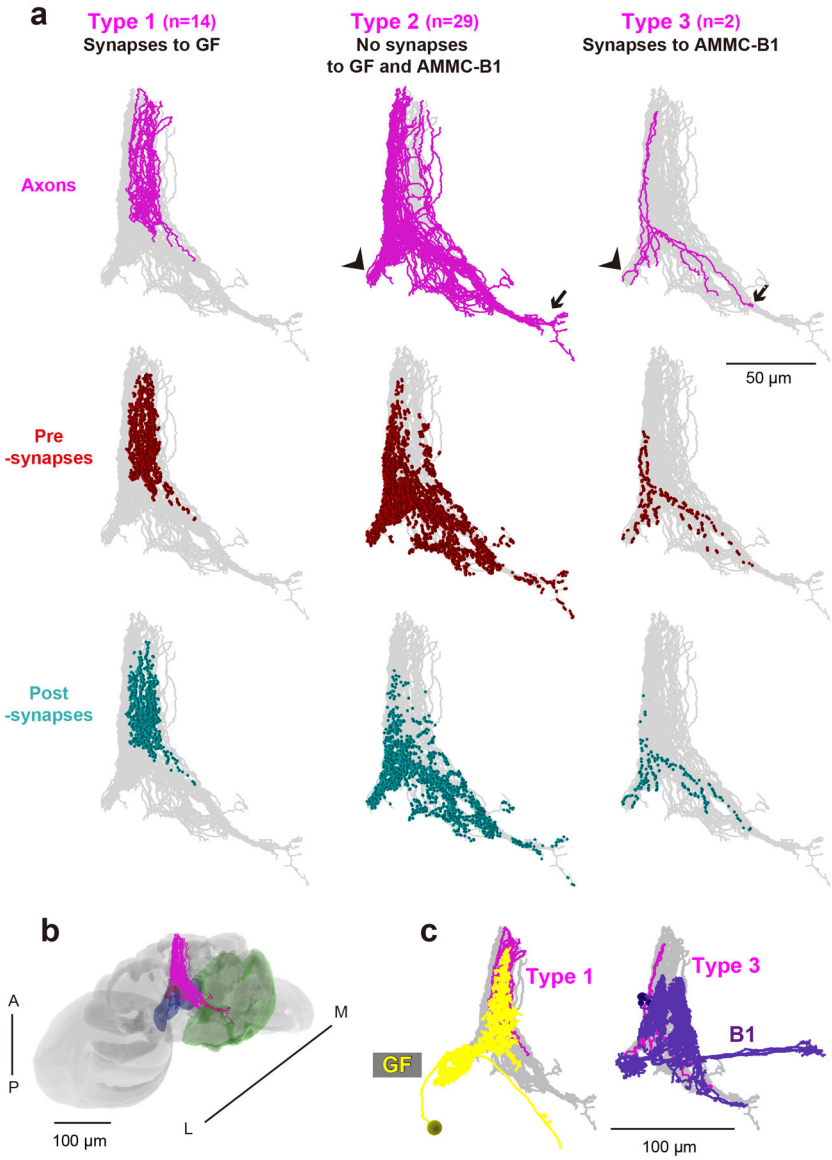

Figure 7 |. Oblique view of three types of JO-A neurons

(a) The color code is the same as that in Figure 6, and the angle is the same as that in Figure 3. The arrow and arrowhead indicate the axons of type- 2 and 3 JO-A neurons innervating the GNG and WED, respectively. (b) Axons of JO-A neurons (magenta) in the brain (gray). The angle of the brain is the same as that in the panel a. WED (blue) and GNG (green) neuropil in the brain are shown. (c) Spatial overlap between the axons of each type of JO-A neurons (magenta) and the neurites of GF (left panel, yellow) or AMMC-B1 neurons (right panel, dark violet). A, anterior; L, lateral; M, medial; P, posterior.

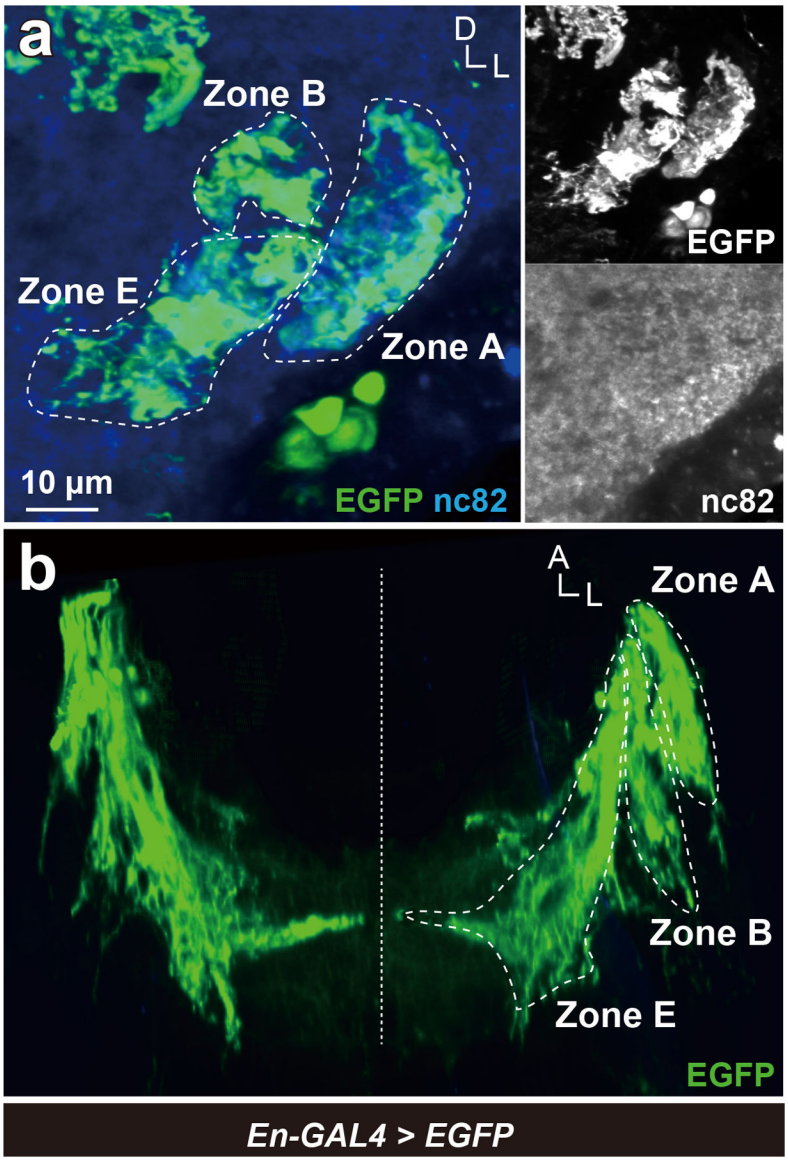

Figure 8 |. *Engrailed-GAL4* expression in JO neurons

(a) *En-GAL4* positive neurons were visualized by expressing EGFP. Axons of JO-A, JO-B, and JO-E neurons were *En-GAL4* positive, whose signals were detected in AMMC zones A, B, and E (green). Nc82 antibodies visualize neuropil in the brain (blue). Frontal view of a ventrolateral side of a central brain is shown. (b) 3D reconstruction of *En-GAL4* positive JO neurons in horizontal view. Signals not relevant to JO neurons were erased manually in panel b for clarity. Dashed horizontal line indicates the midline of the brain. A, anterior; D, dorsal; L, lateral.

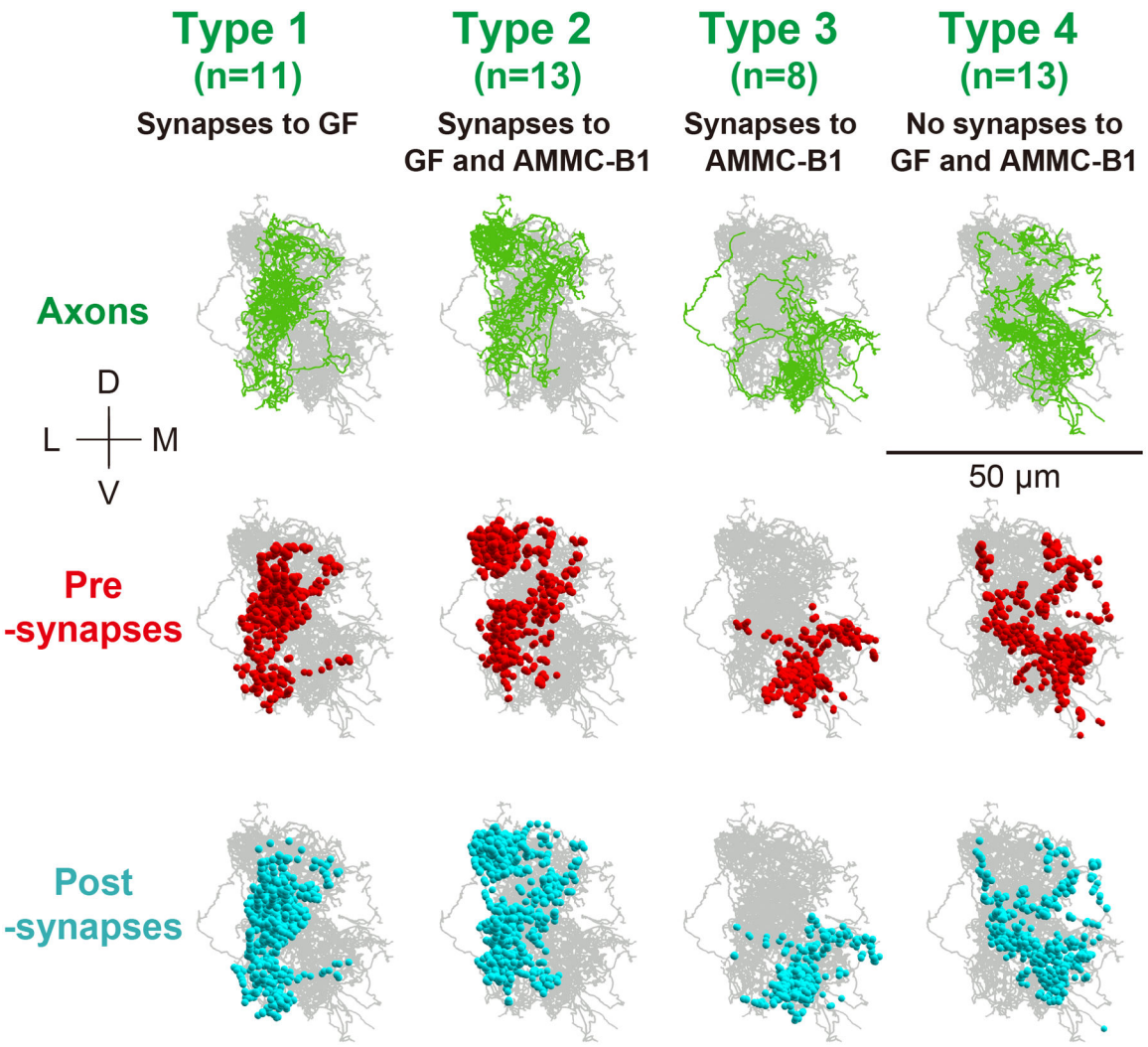

Figure 9 |. Four types of JO-B neurons

Frontal views of axons (green), presynapses (red dots), and postsynapses (light blue dots) are shown. D, dorsal; L, lateral; M, medial; V, ventral.

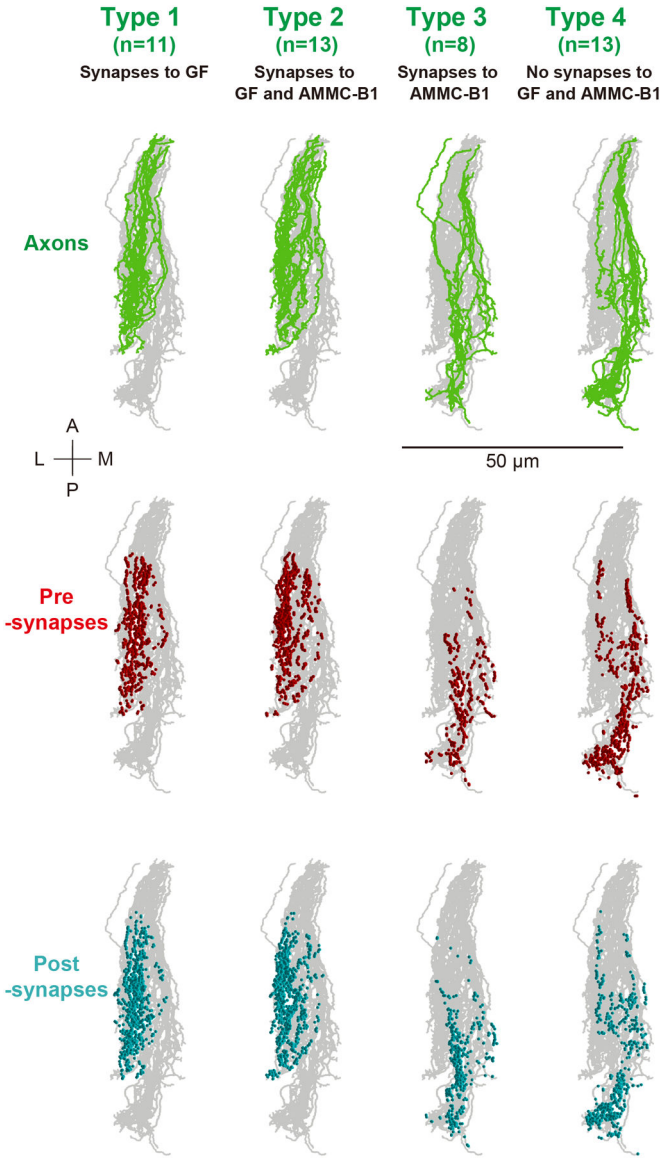

Figure 10 |. Horizontal view of four types of JO-B neurons

The color code is the same as that in Figure 9. A, anterior; L, lateral; M, medial; P, posterior.

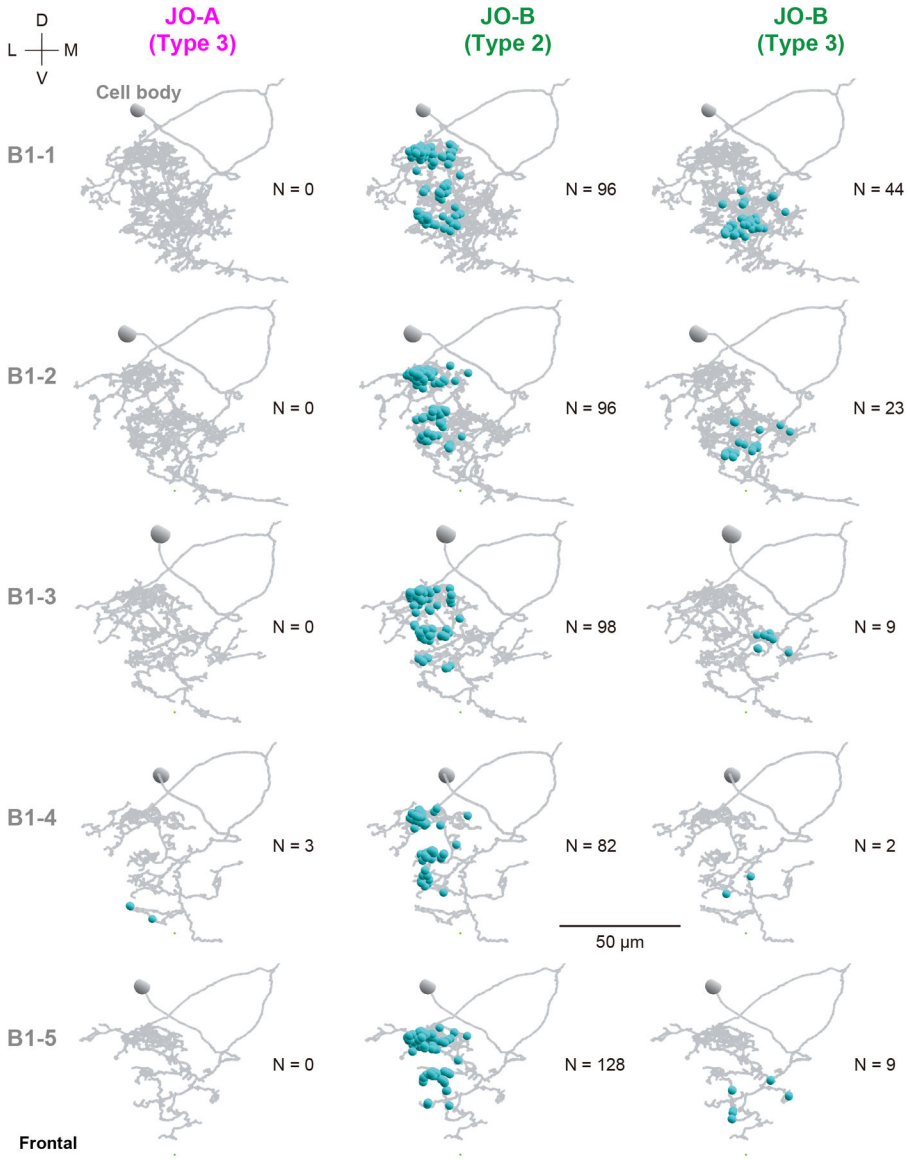

Figure 11 |. Synapse distribution in the dendritic region of AMMC-B1 neurons

Frontal views of synapse distributions (light blue dots) from type-3 JO-A (left), and type- 2 (middle) and 3 JO-B neurons (right) to the dendritic regions of AMMC-B1 neurons (gray) are shown. N at each panel indicates the number of synapses. D, dorsal; L, lateral; M, medial; V, ventral.

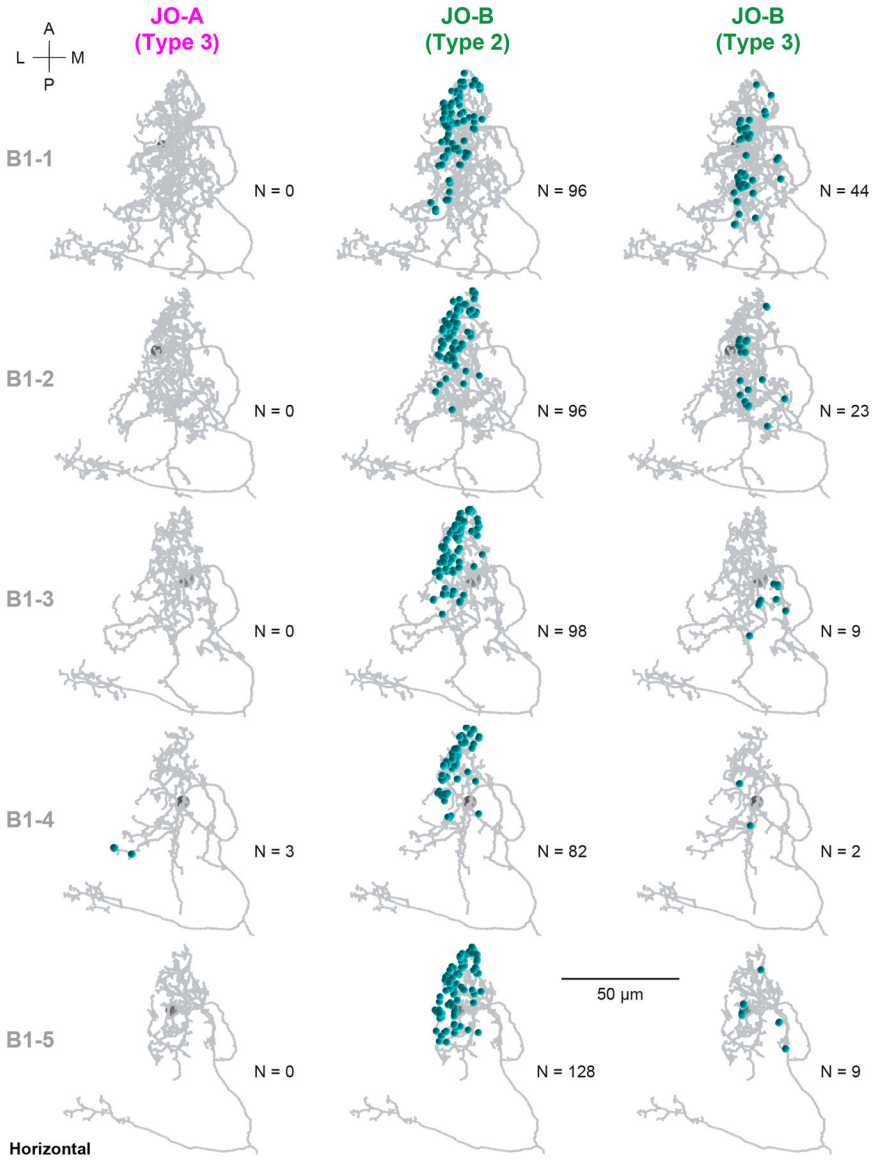

Figure 12 |. Horizontal view of synapse distribution in the dendritic region of AMMC-B1 neurons

The color code is the same as that in Figure 11. A, anterior; L, lateral; M, medial; P, posterior.

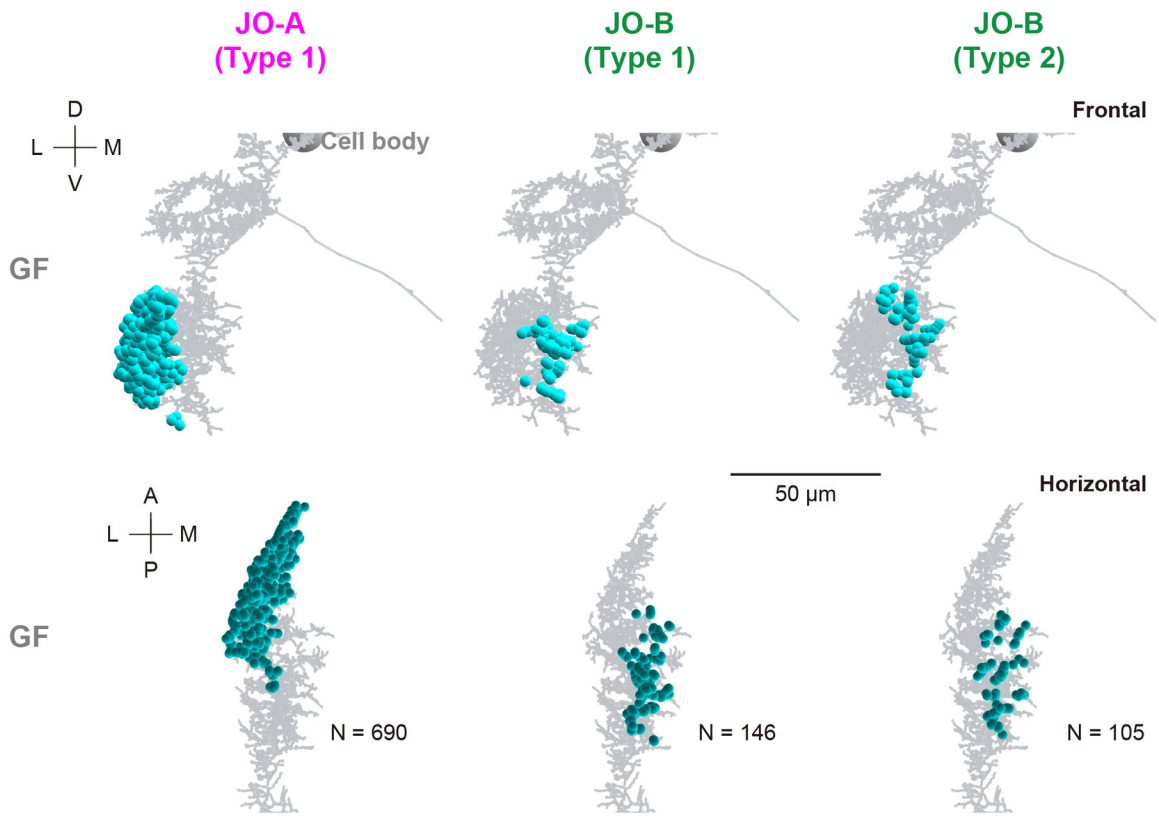

Figure 13 |. Distribution of synapses from JO neurons to the GF neuron

Frontal (top) and horizontal views (bottom) of synapse distributions (light blue dots) from type-1 JO-A (left), and type- 1 (middle) and 2 (right) JO-B neurons to the dendritic regions of GF neuron (gray) are shown. N at the bottom panel indicates the number of synapses. A, anterior; D, dorsal; L, lateral; M, medial; P, posterior; V, ventral.

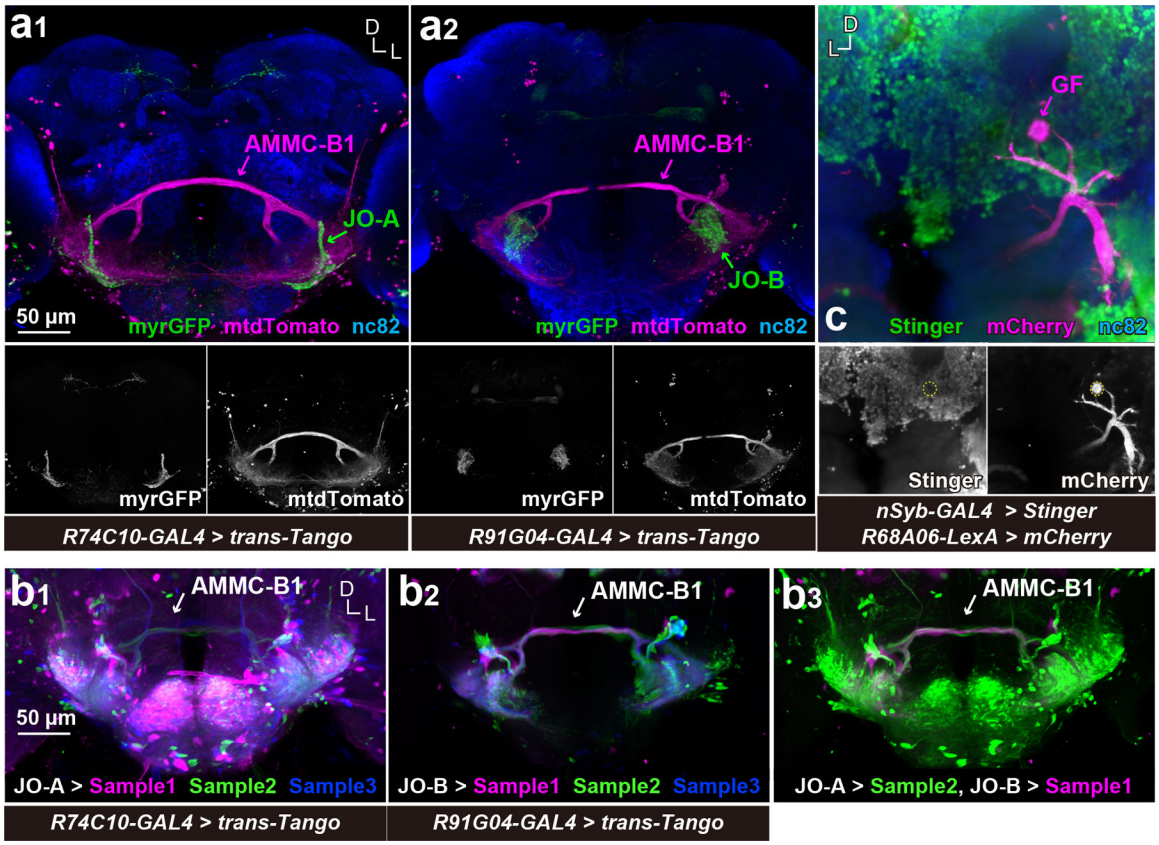

Figure 14 |. *trans*-Tango visualizes neurons postsynaptic of JO-A and JO-B neurons

(a) AMMC-B1 neurons are monosynaptic downstream of JO-A and JO-B neurons. *R74C10-GAL4* (a_1) and *R91G04-GAL4* (a_2) drivers label JO-A and JO-B neurons, respectively (green). *trans*-Tango using these *GAL4* drivers was used to visualize AMMC-B1 neurons (magenta). Nc82 antibodies visualize neuropil in the brain. Stacked images of optical sections are shown, in which anterior and posterior sections of the brain are not included for clarity. (b) *trans*-Tango signals after image registrations. (b_1 and b_2) Three *trans*-Tango brain samples for JO-A (*R74C10-GAL4*) (b_1) and JO-B neurons (*R91G04-GAL4*) (b_2) are shown. Three samples registered to a single brain space are overlaid in different colors. (b_3) Overlay of JO-A and JO-B *trans*-Tango brains. The *trans*-Tango signals of JO-A and JO-B are the same as those in the left (JO-A > Sample 2) and middle panels (JO-B > Sample 1), respectively. (c) GF neuron is devoid of *nSyb-GAL4* signals. GF neuron is labeled using mCherry-HA marker (magenta). Nuclei of *nSyb-GAL4* positive cells are labeled with Stinger, a nuclear-localized GFP marker (green). The cell body of the GF neuron is outlined in the bottom panel. D, dorsal; L, lateral.

Table 1:

Summary of traced JO-A and JO-B neurons

Name	Type	Number of presynapses	Number of postsynapses	Axon length (μm)	Number of presynapses / μm	Number of postsynapses / μm
JO-A-1	1	612	81	162.7	3.76	0.50
JO-A-2		651	84	140.1	4.65	0.60
JO-A-3		546	80	140.7	3.88	0.57
JO-A-4		577	108	179.2	3.22	0.60
JO-A-5		488	83	148.6	3.28	0.56
JO-A-6		519	78	152.9	3.39	0.51
JO-A-7		469	106	164.1	2.86	0.65
JO-A-8		505	78	155.7	3.24	0.50
JO-A-9		532	93	179.2	2.97	0.52
JO-A-10		727	78	179.9	4.04	0.43
JO-A-11		626	103	181.0	3.46	0.57
JO-A-12		492	113	128.7	3.82	0.88
JO-A-13		475	103	154.4	3.08	0.67
JO-A-14		771	91	208.2	3.70	0.44
JO-A-15	2	1012	62	379.2	2.67	0.16
JO-A-16		1288	70	396.8	3.25	0.18
JO-A-17		1330	71	352.8	3.77	0.20
JO-A-18		1010	124	345.2	2.93	0.36
JO-A-19		1249	85	364.1	3.43	0.23
JO-A-20		789	98	248.2	3.18	0.39
JO-A-21		1025	135	329.3	3.11	0.41
JO-A-22		962	141	320.2	3.00	0.44
JO-A-23		873	128	292.0	2.99	0.44
JO-A-24		996	121	326.9	3.05	0.37
JO-A-25		1073	70	353.0	3.04	0.20
JO-A-26		988	143	311.4	3.17	0.46
JO-A-27		977	132	339.0	2.88	0.39
JO-A-28		1111	70	379.6	2.93	0.18
JO-A-29		1217	62	410.7	2.96	0.15
JO-A-30		1124	94	423.3	2.66	0.22
JO-A-31		1225	95	435.8	2.81	0.22
JO-A-32		842	77	284.9	2.96	0.27
JO-A-33		1010	80	346.8	2.91	0.23
JO-A-34		571	48	222.7	2.56	0.22
JO-A-35		516	59	265.7	1.94	0.22
JO-A-36		510	51	243.0	2.10	0.21
JO-A-37		535	43	239.6	2.23	0.18
JO-A-38		1189	81	377.6	3.15	0.21
JO-A-39		737	51	303.6	2.43	0.17

Name	Type	Number of presynapses	Number of postsynapses	Axon length (μm)	Number of presynapses / μm	Number of postsynapses / μm
JO-A-40		1308	111	301.1	4.34	0.37
JO-A-41		1074	112	320.7	3.35	0.35
JO-A-42		2122	108	755.6	2.81	0.14
JO-A-43		1404	126	327.6	4.29	0.38
JO-A-44	3	1169	134	337.3	3.47	0.40
JO-A-45		1082	141	295.9	3.66	0.48
Mean ± SD		896 ± 344	93 ± 27	286.8 ± 114.9	3.1 ± 0.6	0.3 ± 0.17
JO-B-1		268	105	224.6	1.19	0.47
JO-B-2		253	136	236.0	1.07	0.58
JO-B-3		261	113	213.7	1.22	0.53
JO-B-4		270	91	221.4	1.22	0.41
JO-B-5		394	102	155.8	2.53	0.65
JO-B-6	1	222	94	177.7	1.25	0.53
JO-B-7		431	97	140.9	3.06	0.69
JO-B-8		409	93	166.7	2.45	0.56
JO-B-9		379	105	178.8	2.12	0.59
JO-B-10		354	96	162.9	2.17	0.59
JO-B-11		346	68	132.7	2.61	0.51
JO-B-12		482	108	172.2	2.80	0.63
JO-B-13		308	84	182.4	1.69	0.46
JO-B-14		266	86	149.3	1.78	0.58
JO-B-15		299	102	177.9	1.68	0.57
JO-B-16		319	81	116.8	2.73	0.69
JO-B-17		331	83	133.1	2.49	0.62
JO-B-18	2	234	103	170.6	1.37	0.60
JO-B-19		346	115	168.0	2.06	0.68
JO-B-20		299	99	197.5	1.51	0.50
JO-B-21		251	115	235.7	1.07	0.49
JO-B-22		338	95	146.9	2.30	0.65
JO-B-23		356	96	124.4	2.86	0.77
JO-B-24		330	137	241.8	1.36	0.57
JO-B-25		249	65	185.2	1.34	0.35
JO-B-26		203	85	165.9	1.22	0.51
JO-B-27		207	85	175.5	1.18	0.48
JO-B-28	3	217	73	180.6	1.20	0.40
JO-B-29		343	64	188.9	1.82	0.34
JO-B-30		180	52	140.8	1.28	0.37
JO-B-31		259	53	170.5	1.52	0.31
JO-B-32		619	48	222.1	2.79	0.22
JO-B-33	4	428	65	206.2	2.08	0.32
JO-B-34		525	79	206.8	2.54	0.38

Name	Type	Number of presynapses	Number of postsynapses	Axon length (μm)	Number of presynapses / μm	Number of postsynapses / μm
JO-B-35		342	56	175.4	1.95	0.32
JO-B-36		379	29	214.1	1.77	0.14
JO-B-37		330	36	169.3	1.95	0.21
JO-B-38		382	44	152.9	2.50	0.29
JO-B-39		316	38	165.9	1.90	0.23
JO-B-40		354	35	179.5	1.97	0.19
JO-B-41		437	86	214.5	2.04	0.40
JO-B-42		234	37	156.5	1.49	0.24
JO-B-43		316	55	130.6	2.42	0.42
JO-B-44		314	69	175.6	1.79	0.39
JO-B-45		428	104	170.7	2.51	0.61
Mean ± SD		329 ± 89	81 ± 27	177.2 ± 31.2	1.9 ± 0.6	0.5 ± 0.16

Table 2:

Number of JO neurons that synapse with other JO neurons

JO neurons	Number of traced neurons	Axon length (μm)	Number of synapses		Neurons that synapse with other JO-A or JO-B neurons	
			Pre	Post	JO-A neurons	JO-B neurons
JO-A	45	286.8 ± 114.9	896 ± 344	93 ± 27	13 (29%)	0 (0%)
JO-B	45	177.2 ± 31.2	329 ± 89	81 ± 27	0 (0%)	21 (47%)

Numbers in the bracket indicate percentages.

Table 3:

Presynapses of each JO-A neuron

Name	Type	All synapses	To JO-A	To B1-4	To GF	To unidentified	To JO-A (%)	To B1-4 (%)	To GF (%)	To unidentified (%)
JO-A-1	1	612	0	0	69	543	0	0	11.27	88.73
JO-A-2		651	0	0	63	588	0	0	9.68	90.32
JO-A-3		546	1	0	59	486	0.18	0	10.81	89.01
JO-A-4		577	1	0	56	520	0.17	0	9.71	90.12
JO-A-5		488	0	0	56	432	0	0	11.48	88.52
JO-A-6		519	1	0	48	470	0.19	0	9.25	90.56
JO-A-7		469	2	0	46	421	0.43	0	9.81	89.77
JO-A-8		505	1	0	45	459	0.20	0	8.91	90.89
JO-A-9		532	0	0	45	487	0	0	8.46	91.54
JO-A-10		727	2	0	45	680	0.28	0	6.19	93.54
JO-A-11		626	0	0	44	582	0	0	7.03	92.97
JO-A-12		492	1	0	42	449	0.20	0	8.54	91.26
JO-A-13		475	0	0	39	436	0	0	8.21	91.79
JO-A-14		771	1	0	33	737	0.13	0	4.28	95.59
JO-A-15	2	1012	0	0	0	1012	0	0	0	100
JO-A-16		1288	1	0	0	1287	0.08	0	0	99.92
JO-A-17		1330	1	0	0	1329	0.08	0	0	99.92
JO-A-18		1010	0	0	0	1010	0	0	0	100
JO-A-19		1249	0	0	0	1249	0	0	0	100
JO-A-20		789	0	0	0	789	0	0	0	100
JO-A-21		1025	0	0	0	1025	0	0	0	100
JO-A-22		962	0	0	0	962	0	0	0	100
JO-A-23		873	0	0	0	873	0	0	0	100
JO-A-24		996	0	0	0	996	0	0	0	100
JO-A-25		1073	1	0	0	1072	0.09	0	0	99.91
JO-A-26		988	0	0	0	988	0	0	0	100
JO-A-27		977	0	0	0	977	0	0	0	100
JO-A-28		1111	0	0	0	1111	0	0	0	100
JO-A-29		1217	0	0	0	1217	0	0	0	100
JO-A-30		1124	1	0	0	1123	0.09	0	0	99.91
JO-A-31		1225	0	0	0	1225	0	0	0	100
JO-A-32		842	0	0	0	842	0	0	0	100
JO-A-33		1010	0	0	0	1010	0	0	0	100
JO-A-34		571	0	0	0	571	0	0	0	100
JO-A-35		516	0	0	0	516	0	0	0	100
JO-A-36		510	0	0	0	510	0	0	0	100
JO-A-37		535	1	0	0	534	0.19	0	0	99.81
JO-A-38		1189	0	0	0	1189	0	0	0	100
JO-A-39		737	0	0	0	737	0	0	0	100

Name	Type	All synapses	To JO-A	To B1-4	To GF	To unidentified	To JO-A (%)	To B1-4 (%)	To GF (%)	To unidentified (%)
JO-A-40		1308	0	0	0	1308	0	0	0	100
JO-A-41		1074	0	0	0	1074	0	0	0	100
JO-A-42		2122	0	0	0	2122	0	0	0	100
JO-A-43		1404	0	0	0	1404	0	0	0	100
JO-A-44	3	1169	0	2	0	1167	0	0.17	0	99.83
JO-A-45		1082	0	1	0	1081	0	0.09	0	99.91
Total		40,308	15	3	690	39,600	⁄	⁄	⁄	⁄

B1–4, AMMC-B1–4 neuron; Unidentified, unidentified neurons.

Table 4:

Postsynapses of each JO-A neuron

Name	Type	All synapses	From JO-A	From unidentified	From JO-A (%)	From unidentified (%)
JO-A-1	1	81	0	81	0.00	100.00
JO-A-2		84	0	84	0.00	100.00
JO-A-3		80	0	80	0.00	100.00
JO-A-4		108	3	105	2.78	97.22
JO-A-5		83	0	83	0.00	100.00
JO-A-6		78	0	78	0.00	100.00
JO-A-7		106	1	105	0.94	99.06
JO-A-8		78	0	78	0.00	100.00
JO-A-9		93	0	93	0.00	100.00
JO-A-10		78	1	77	1.28	98.72
JO-A-11		103	3	100	2.91	97.09
JO-A-12		113	0	113	0.00	100.00
JO-A-13		103	0	103	0.00	100.00
JO-A-14		91	2	89	2.20	97.80
JO-A-15	2	62	0	62	0.00	100.00
JO-A-16		70	0	70	0.00	100.00
JO-A-17		71	0	71	0.00	100.00
JO-A-18		124	0	124	0.00	100.00
JO-A-19		85	1	84	1.18	98.82
JO-A-20		98	0	98	0.00	100.00
JO-A-21		135	0	135	0.00	100.00
JO-A-22		141	0	141	0.00	100.00
JO-A-23		128	0	128	0.00	100.00
JO-A-24		121	0	121	0.00	100.00
JO-A-25		70	1	69	1.43	98.57
JO-A-26		143	0	143	0.00	100.00
JO-A-27		132	0	132	0.00	100.00
JO-A-28		70	1	69	1.43	98.57
JO-A-29		62	0	62	0.00	100.00
JO-A-30		94	0	94	0.00	100.00
JO-A-31		95	0	95	0.00	100.00
JO-A-32		77	0	77	0.00	100.00
JO-A-33		80	0	80	0.00	100.00
JO-A-34		48	0	48	0.00	100.00
JO-A-35		59	0	59	0.00	100.00
JO-A-36		51	1	50	1.96	98.04
JO-A-37		43	0	43	0.00	100.00
JO-A-38		81	0	81	0.00	100.00
JO-A-39		51	1	50	1.96	98.04

Name	Type	All synapses	From JO-A	From unidentified	From JO-A (%)	From unidentified (%)
JO-A-40		111	0	111	0.00	100.00
JO-A-41		112	0	112	0.00	100.00
JO-A-42		108	0	108	0.00	100.00
JO-A-43		126	0	126	0.00	100.00
JO-A-44	3	134	0	134	0.00	100.00
JO-A-45		141	0	141	0.00	100.00
Total		4,202	15	4,187	⁄	⁄

Table 5:

Presynapses of each JO-B neuron

Name	Type	All synapses	To JO-B	To B1-1	To B1-2	To B1-3	To B1-4	To B1-5	To GF	To unidentified
JO-B-1		268	1	0	0	0	0	0	39	228
JO-B-2		253	0	0	0	0	0	0	37	216
JO-B-3		261	1	0	0	0	0	0	31	229
JO-B-4		270	4	0	0	0	0	0	24	242
JO-B-5		394	0	0	0	0	0	0	4	390
JO-B-6	1	222	0	0	0	0	0	0	3	219
JO-B-7		431	2	0	0	0	0	0	2	427
JO-B-8		409	1	0	0	0	0	0	2	406
JO-B-9		379	2	0	0	0	0	0	2	375
JO-B-10		354	0	0	0	0	0	0	1	353
JO-B-11		346	1	0	0	0	0	0	1	344
JO-B-12		482	0	9	14	35	26	22	1	375
JO-B-13		308	0	13	8	6	3	9	1	268
JO-B-14		266	0	9	13	13	9	17	3	202
JO-B-15		299	0	12	12	10	15	19	2	229
JO-B-16		319	1	7	9	8	10	16	3	265
JO-B-17		331	0	8	5	8	7	22	1	280
JO-B-18	2	234	0	11	6	6	3	6	17	185
JO-B-19		346	1	7	11	7	1	8	15	296
JO-B-20		299	3	16	12	4	7	7	15	235
JO-B-21		251	0	4	1	1	1	2	1	241
JO-B-22		338	0	0	2	0	0	0	1	335
JO-B-23		356	1	0	1	0	0	0	2	352
JO-B-24		330	0	0	2	0	0	0	43	285
JO-B-25		249	0	6	2	9	1	5	0	226
JO-B-26		203	0	13	6	0	1	2	0	181
JO-B-27		207	2	8	6	0	0	2	0	189
JO-B-28	3	217	1	2	2	0	0	0	0	212
JO-B-29		343	0	1	1	0	0	0	0	341
JO-B-30		180	1	11	5	0	0	0	0	163
JO-B-31		259	1	2	1	0	0	0	0	255
JO-B-32		619	1	1	0	0	0	0	0	617
JO-B-33		428	0	0	0	0	0	0	0	428
JO-B-34		525	2	0	0	0	0	0	0	523
JO-B-35		342	1	0	0	0	0	0	0	341
JO-B-36	4	379	1	0	0	0	0	0	0	378
JO-B-37		330	1	0	0	0	0	0	0	329
JO-B-38		382	0	0	0	0	0	0	0	382
JO-B-39		316	0	0	0	0	0	0	0	316

Name	Type	All synapses	To JO-B	To B1-1	To B1-2	To B1-3	To B1-4	To B1-5	To GF	To unidentified
JO-B-40		354	0	0	0	0	0	0	0	354
JO-B-41		437	1	0	0	0	0	0	0	436
JO-B-42		234	0	0	0	0	0	0	0	234
JO-B-43		316	0	0	0	0	0	0	0	316
JO-B-44		314	0	0	0	0	0	0	0	314
JO-B-45		428	0	0	0	0	0	0	0	428
Total		14,808	30	140	119	107	84	137	251	13,940

Table 6:

The percentage of presynapses of each JO-B neuron

Name	Type	To JO-B (%)	To B1-1 (%)	To B1-2 (%)	To B1-3 (%)	To B1-4 (%)	To B1-5 (%)	To GF (%)	To unidentified (%)
JO-B-1		0.37	0	0	0	0	0	14.55	85.07
JO-B-2		0	0	0	0	0	0	14.62	85.38
JO-B-3		0.38	0	0	0	0	0	11.88	87.74
JO-B-4		1.48	0	0	0	0	0	8.89	89.63
JO-B-5		0	0	0	0	0	0	1.02	98.98
JO-B-6	1	0	0	0	0	0	0	1.35	98.65
JO-B-7		0.46	0	0	0	0	0	0.46	99.07
JO-B-8		0.24	0	0	0	0	0	0.49	99.27
JO-B-9		0.53	0	0	0	0	0	0.53	98.94
JO-B-10		0	0	0	0	0	0	0.28	99.72
JO-B-11		0.29	0	0	0	0	0	0.29	99.42
JO-B-12		0	1.87	2.90	7.26	5.39	4.56	0.21	77.80
JO-B-13		0	4.22	2.60	1.95	0.97	2.92	0.32	87.01
JO-B-14		0	3.38	4.89	4.89	3.38	6.39	1.13	75.94
JO-B-15		0	4.01	4.01	3.34	5.02	6.35	0.67	76.59
JO-B-16		0.31	2.19	2.82	2.51	3.13	5.02	0.94	83.07
JO-B-17		0	2.42	1.51	2.42	2.11	6.65	0.30	84.59
JO-B-18	2	0	4.70	2.56	2.56	1.28	2.56	7.26	79.06
JO-B-19		0.29	2.02	3.18	2.02	0.29	2.31	4.34	85.55
JO-B-20		1.00	5.35	4.01	1.34	2.34	2.34	5.02	78.60
JO-B-21		0	1.59	0.40	0.40	0.40	0.80	0.40	96.02
JO-B-22		0	0	0.59	0	0	0	0.30	99.11
JO-B-23		0.28	0	0.28	0	0	0	0.56	98.88
JO-B-24		0	0	0.61	0	0	0	13.03	86.36
JO-B-25		0	2.41	0.80	3.61	0.40	2.01	0	90.76
JO-B-26		0	6.40	2.96	0	0.49	0.99	0	89.16
JO-B-27		0.97	3.86	2.90	0	0	0.97	0	91.30
JO-B-28	3	0.46	0.92	0.92	0	0	0	0	97.70
JO-B-29		0	0.29	0.29	0	0	0	0	99.42
JO-B-30		0.56	6.11	2.78	0	0	0	0	90.56
JO-B-31		0.39	0.77	0.39	0	0	0	0	98.46
JO-B-32		0.16	0.16	0	0	0	0	0	99.68
JO-B-33		0	0	0	0	0	0	0	100
JO-B-34		0.38	0	0	0	0	0	0	99.62
JO-B-35		0.29	0	0	0	0	0	0	99.71
JO-B-36	4	0.26	0	0	0	0	0	0	99.74
JO-B-37		0.30	0	0	0	0	0	0	99.70
JO-B-38		0	0	0	0	0	0	0	100

Name	Type	To JO-B (%)	To B1-1 (%)	To B1-2 (%)	To B1-3 (%)	To B1-4 (%)	To B1-5 (%)	To GF (%)	To unidentified (%)
JO-B-39		0	0	0	0	0	0	0	100
JO-B-40		0	0	0	0	0	0	0	100
JO-B-41		0.23	0	0	0	0	0	0	99.77
JO-B-42		0	0	0	0	0	0	0	100
JO-B-43		0	0	0	0	0	0	0	100
JO-B-44		0	0	0	0	0	0	0	100
JO-B-45		0	0	0	0	0	0	0	100

Table 7:

Postsynapses of each JO-B neuron

Name	Type	All synapses	From JO-B	From unidentified	From JO-B (%)	From unidentified (%)
JO-B-1		105	1	104	0.95	99.05
JO-B-2		136	0	136	0	100
JO-B-3		113	4	109	3.54	96.46
JO-B-4		91	1	90	1.10	98.90
JO-B-5		102	1	101	0.98	99.02
JO-B-6	1	94	0	94	0	100
JO-B-7		97	0	97	0	100
JO-B-8		93	1	92	1.08	98.92
JO-B-9		105	0	105	0	100
JO-B-10		96	0	96	0	100
JO-B-11		68	0	68	0	100
JO-B-12		108	1	107	0.93	99.07
JO-B-13		84	0	84	0	100
JO-B-14		86	3	83	3.49	96.51
JO-B-15		102	0	102	0	100
JO-B-16		81	0	81	0	100
JO-B-17		83	0	83	0	100
JO-B-18	2	103	1	102	0.97	99.03
JO-B-19		115	0	115	0	100
JO-B-20		99	0	99	0	100
JO-B-21		115	0	115	0	100
JO-B-22		95	1	94	1.05	98.95
JO-B-23		96	1	95	1.04	98.96
JO-B-24		137	1	136	0.73	99.27
JO-B-25		65	0	65	0	100
JO-B-26		85	2	83	2.35	97.65
JO-B-27		85	1	84	1.18	98.82
JO-B-28	3	73	2	71	2.74	97.26
JO-B-29		64	0	64	0	100
JO-B-30		52	0	52	0	100
JO-B-31		53	0	53	0	100
JO-B-32		48	1	47	2.08	97.92
JO-B-33		65	2	63	3.08	96.92
JO-B-34		79	0	79	0	100
JO-B-35		56	1	55	1.79	98.21
JO-B-36	4	29	0	29	0	100
JO-B-37		36	1	35	2.78	97.22
JO-B-38		44	0	44	0	100
JO-B-39		38	1	37	2.63	97.37

Name	Type	All synapses	From JO-B	From unidentified	From JO-B (%)	From unidentified (%)
JO-B-40		35	1	34	2.86	97.14
JO-B-41		86	0	86	0	100
JO-B-42		37	0	37	0	100
JO-B-43		55	0	55	0	100
JO-B-44		69	0	69	0	100
JO-B-45		104	2	102	1.92	98.08
Total		3,662	30	3,632	⁄	⁄

Table 8:

Summary of traced AMMC-B1 neurons

		AMMC-B1					
		1	**2**	**3**	**4**	**5**	**Mean ± SD**
Number of branches		983	731	440	280	302	547.2 ± 302.8
Neurite length (mm)		3.54	2.75	2.12	1.54	1.38	2.27 ± 0.89
Number of postsynapses	from JO-A	0	0	0	3	0	0.8 ± 1.3
	from JO-B	140	119	107	84	137	117 ± 23.0
	Total	140	119	107	87	137	118 ± 22.0

Table 9:

Synapses from JO-A and JO-B neuron axons to AMMC-B1 and GF neurons

JO-A	Type	AMMC-B1					GF	JO-B	Type	AMMC-B1					GF
		1	2	3	4	5				1	2	3	4	5	
JO-A-1	1	0	0	0	0	0	69	JO-B-1	1	0	0	0	0	0	39
JO-A-2		0	0	0	0	0	63	JO-B-2		0	0	0	0	0	37
JO-A-3		0	0	0	0	0	59	JO-B-3		0	0	0	0	0	31
JO-A-4		0	0	0	0	0	56	JO-B-4		0	0	0	0	0	24
JO-A-5		0	0	0	0	0	56	JO-B-5		0	0	0	0	0	4
JO-A-6		0	0	0	0	0	48	JO-B-6		0	0	0	0	0	3
JO-A-7		0	0	0	0	0	46	JO-B-7		0	0	0	0	0	2
JO-A-8		0	0	0	0	0	45	JO-B-8		0	0	0	0	0	2
JO-A-9		0	0	0	0	0	45	JO-B-9		0	0	0	0	0	2
JO-A-10		0	0	0	0	0	45	JO-B-10		0	0	0	0	0	1
JO-A-11		0	0	0	0	0	44	JO-B-11		0	0	0	0	0	1
JO-A-12		0	0	0	0	0	42	JO-B-12		9	14	35	26	22	1
JO-A-13		0	0	0	0	0	39	JO-B-13		13	8	6	3	9	1
JO-A-14		0	0	0	0	0	33	JO-B-14		9	13	13	9	17	3
JO-A-15	2	0	0	0	0	0	0	JO-B-15		12	12	10	15	19	2
JO-A-16		0	0	0	0	0	0	JO-B-16		7	9	8	10	16	3
JO-A-17		0	0	0	0	0	0	JO-B-17		8	5	8	7	22	1
JO-A-18		0	0	0	0	0	0	JO-B-18	2	11	6	6	3	6	17
JO-A-19		0	0	0	0	0	0	JO-B-19		7	11	7	1	8	15
JO-A-20		0	0	0	0	0	0	JO-B-20		16	12	4	7	7	15
JO-A-21		0	0	0	0	0	0	JO-B-21		4	1	1	1	2	1
JO-A-22		0	0	0	0	0	0	JO-B-22		0	2	0	0	0	1
JO-A-23		0	0	0	0	0	0	JO-B-23		0	1	0	0	0	2
JO-A-24		0	0	0	0	0	0	JO-B-24		0	2	0	0	0	43
JO-A-25		0	0	0	0	0	0	JO-B-25		6	2	9	1	5	0
JO-A-26		0	0	0	0	0	0	JO-B-26		13	6	0	1	2	0
JO-A-27		0	0	0	0	0	0	JO-B-27		8	6	0	0	2	0
JO-A-28		0	0	0	0	0	0	JO-B-28	3	2	2	0	0	0	0
JO-A-29		0	0	0	0	0	0	JO-B-29		1	1	0	0	0	0
JO-A-30		0	0	0	0	0	0	JO-B-30		11	5	0	0	0	0
JO-A-31		0	0	0	0	0	0	JO-B-31		2	1	0	0	0	0
JO-A-32		0	0	0	0	0	0	JO-B-32		1	0	0	0	0	0
JO-A-33		0	0	0	0	0	0	JO-B-33		0	0	0	0	0	0
JO-A-34		0	0	0	0	0	0	JO-B-34		0	0	0	0	0	0
JO-A-35		0	0	0	0	0	0	JO-B-35		0	0	0	0	0	0
JO-A-36		0	0	0	0	0	0	JO-B-36	4	0	0	0	0	0	0
JO-A-37		0	0	0	0	0	0	JO-B-37		0	0	0	0	0	0
JO-A-38		0	0	0	0	0	0	JO-B-38		0	0	0	0	0	0

JO-A	Type	AMMC-B1					GF	JO-B	Type	AMMC-B1					GF
		1	2	3	4	5				1	2	3	4	5	
JO-A-39		0	0	0	0	0	0	JO-B-39		0	0	0	0	0	0
JO-A-40		0	0	0	0	0	0	JO-B-40		0	0	0	0	0	0
JO-A-41		0	0	0	0	0	0	JO-B-41		0	0	0	0	0	0
JO-A-42		0	0	0	0	0	0	JO-B-42		0	0	0	0	0	0
JO-A-43		0	0	0	0	0	0	JO-B-43		0	0	0	0	0	0
JO-A-44	3	0	0	0	2	0	0	JO-B-44		0	0	0	0	0	0
JO-A-45		0	0	0	1	0	0	JO-B-45		0	0	0	0	0	0
Total		0	0	0 (3)	3	0	690	Total		140	119	107 (587)	84	137	251

The color code represents the number of synapses. The darker the color, the more synaptic connections they have (magenta for JO-A and green for JO-B). The number in the parenthesis shows the sum of the five AMMC-B1 neurons.

Table 10:

Total number of synapses in each type of JO-A and JO-B neuron axons

JO-A types	Number of synapses in JO-A neurons		Number of synapses with other JO-A neurons		
	Pre	Post	Type 1	Type 2	Type 3
Type 1 (n=14)	7,990	1,279	10	0	0
Type 2 (n=29)	30,067	2,648	0	5	0
Type 3 (n=2)	2,251	275	0	0	0
Total (n=45)	40,308	4,202	15		

JO-B types	Number of synapses in JO-B neurons		Number of synapses with other JO-B neurons			
	Pre	Post	Type 1	Type 2	Type 3	Type 4
Type 1 (n=11)	3,587	1,100	8	2	0	2
Type 2 (n=13)	4,159	1,304	0	6	0	0
Type 3 (n=8)	2,277	525	0	0	4	2
Type 4 (n=13)	4,785	733	0	0	1	5
Total (n=45)	14,808	3,662	30			

Table 11:

Number of synapses between JO-A neurons

Type 1		To				
		JO-A-4	JO-A-7	JO-A-10	JO-A-11	JO-A-14
From	JO-A-3	1	0	0	0	0
	JO-A-4	0	1	0	0	0
	JO-A-6	1	0	0	0	0
	JO-A-7	1	0	0	1	0
	JO-A-8	0	0	0	1	0
	JO-A-10	0	0	0	0	2
	JO-A-12	0	0	0	1	0
	JO-A-14	0	0	1	0	0
Type 2		**To**				
		JO-A-19	**JO-A-25**	**JO-A-28**	**JO-A-36**	**JO-A-39**
From	JO-A-16	0	0	1	0	0
	JO-A-17	1	0	0	0	0
	JO-A-25	0	0	0	0	1
	JO-A-30	0	1	0	0	0
	JO-A-37	0	0	0	1	0

Table 12:

Comparisons between types in JO-A and JO-B neurons

JO-A	Type1 (n = 14)	Type2 (n = 29)	Type3 (n = 2)
Axon length (μm)	136.7 ± 21.5	323.0 ± 100.8	301.3 ± 30.3
Depth (μm)	103.8 ± 6.2	145.8 ± 9.2	139.6 ± 4.7
Presynaptic sites	570.7 ± 95.0	1036.8 ± 323.8	1125.5 ± 61.5
Postsynaptic sites	91.4 ± 12.8	91.3 ± 31.0	137.5 ± 4.9

JO-B	Type1 (n = 11)	Type2 (n = 13)	Type3 (n = 8)	Type4 (n = 13)
Axon length (μm)	156.0 ± 39.4	146.1 ± 37.9	163.4 ± 29.1	164.2 ± 31.8
Depth (μm)	112.0 ± 8.5	111.3 ± 8.0	136.9 ± 9.7	135.0 ± 19.2
Presynaptic sites	326.1 ± 73.1	319.9 ± 61.1	284.6 ± 144.1	368.1 ± 73.9
Postsynaptic sites	100.0 ± 16.5	100.3 ± 15.9	65.6 ± 14.5	56.4 ± 23.6

Depth (μm) indicates the distance between the most frontal section of the brain (i.e., section #1) and the most posterior section innervated by each JO neuron.

Table 13:

Number of synapses between JO neurons and unidentified neurons

JO-A	Type 1	Type 2	Type 3
Presynapses	520.7 ± 96.0	1036.6 ± 323.8	1124.0 ± 60.8
Postsynapses	90.6 ± 12.3	91.1 ± 31.1	137.5 ± 5.0

JO-B	Type 1	Type 2	Type 3	Type 4
Presynapses	311.7 ± 84.6	272.9 ± 56.6	273 ± 149.7	367.6 ± 73.5
Postsynapses	99.3 ± 16.3	99.7 ± 16.0	64.9 ± 13.9	55.8 ± 22.9

Mean ± standard deviation are shown.

Table 14:

Number of synapses between JO-B neurons

Type 1		To				
		JO-B-1	JO-B-3	JO-B-4	JO-B-5	JO-B-8
From	JO-B-1	0	0	1	0	0
	JO-B-4	1	3	0	0	0
	JO-B-8	0	0	0	1	0
	JO-B-9	0	0	0	0	1
	JO-B-11	0	1	0	0	0

Type 2		To			
		JO-B-14	JO-B-12	JO-B-18	JO-B-22
From	JO-B-16	1	0	0	0
	JO-B-19	0	0	1	0
	JO-B-20	2	1	0	0
	JO-B-23	0	0	0	1

Type 3		To		
		JO-B-26	JO-B-27	JO-B-28
From	JO-B-27	2	0	0
	JO-B-28	0	1	0
	JO-B-30	0	0	1
	JO-B-31	0	0	1

Type 4		To			
		JO-B-33	JO-B-35	JO-B-37	JO-B-39
From	JO-B-34	1	1	0	0
	JO-B-35	1	0	0	0
	JO-B-36	0	0	0	1
	JO-B-41	0	0	1	0

Across types		To				
		JO-B-23	JO-B-24	JO-B-32	JO-B-40	JO-B-45
From	JO-B-3	0	1	0	0	0
	JO-B-7	0	0	0	0	2
	JO-B-9	1	0	0	0	0
	JO-B-32	0	0	0	1	0
	JO-B-37	0	0	1	0	0

Table 15:

Number of synapses from JO-B neurons to AMMC-B1 and GF neurons

JO-B type	AMMC-B1						GF
	1	2	3	4	5	Total	
Type 1	0	0	0	0	0	0	146
Type 2	96	96	98	82	128	500	105
Type 3	44	23	9	2	9	87	0
Type 4	0	0	0	0	0	0	0
Total	140	119	107	84	137	587	251

Numbers of synapses from each type of JO-B neurons to each AMMC-B1 or GF neuron are shown. The darker the color, the more synaptic connections each combination has (green).